Exergy and exergo-economic analysis of a hybrid renewable energy system under different climate conditions

Sonja Kallio, Monica Siroux

▶ **To cite this version:**

Sonja Kallio, Monica Siroux. Exergy and exergo-economic analysis of a hybrid renewable energy system under different climate conditions. Renewable Energy, 2022, 194, pp.396-414. 10.1016/j.renene.2022.05.115 . hal-03991573

HAL Id: hal-03991573
https://hal.science/hal-03991573v1

Submitted on 22 Jul 2024

HAL is a multi-disciplinary open access archive for the deposit and dissemination of scientific research documents, whether they are published or not. The documents may come from teaching and research institutions in France or abroad, or from public or private research centers.

L'archive ouverte pluridisciplinaire **HAL**, est destinée au dépôt et à la diffusion de documents scientifiques de niveau recherche, publiés ou non, émanant des établissements d'enseignement et de recherche français ou étrangers, des laboratoires publics ou privés.

Distributed under a Creative Commons Attribution - NonCommercial 4.0 International License

Version of Record: https://www.sciencedirect.com/science/article/pii/S0960148122007662
Manuscript_7871e1e1f00c28ba857ed77bafbf4a9d

Article

Exergy and Exergo-economic analysis of a hybrid renewable energy system under different climate conditions

Sonja Kallio[1] and Monica Siroux[1*]

[1] *INSA Strasbourg ICUBE University of Strasbourg, Strasbourg, France; sonja.kallio@insa-strasbourg.fr*
* Correspondence: monica.siroux@insa-strasbourg.fr; Tel.: +33388144753

Received: date; Accepted: date; Published: date

Abstract:
The building sector has a great potential to accelerate the decarbonisation by using high efficient and 100% renewable energy production on-site. This allows also increased energy autonomy to protect building owners against increasing electricity prices. The key solution is to apply micro combined heat and power (micro-CHP) systems to form a domestic hybrid renewable energy system (HRES) which supports fluctuating solar energy production by the controllable biomass-fuelled micro-CHP. However, despite the market availability of the technology, the initial investment of such a system is assumed to be a barrier to penetration. In this study, dynamic exergy and exergo-economic analyses of the HRES are conducted in Matlab/Simulink to define the specific costs of energy products when the market available system is applied to the European building stock under different climate and economic conditions. The overall exergy efficiency of the system is 13%-16%. The specific costs have high variation on a monthly and location basis. On a yearly basis, the lowest specific cost of electricity is 0.29 €/kWh in the southernmost location and of heat products 0.319 €/kWh$_{ex}$ (0.034 €/kWh). The comparative results show that the HRES is economically viable and reduces primary energy use and costly irreversibility up to 95%.

Keywords: Hybrid renewable energy systems; Climate conditions; Exergy analysis; Exergo-economics; Renewable micro-cogeneration

Nomenclature

A	area, m^2
a	annuity factor
$\dot{C}$	cost rate, €/h
c	specific cost, €/kWh
c_p	specific heat, J/(kg K)
CRF	Capital Recovery Factor
E	electrical energy, kWh
EL	energy level
$\dot{E}x$	exergy rate, kW
Ex	exergy, kWh
H	enthalpy, kJ
h	specific enthalpy, J/kg
I	component specific initial investment, €
i	interest rate
Ir	irreversibility, W
LHV	lower heating value
m	mass, kg
MC	thermal capacity, J/K
n	lifetime, year
NPV	Net Present Value
OM	operating and maintenance

© 2022 published by Elsevier. This manuscript is made available under the CC BY NC user license
https://creativecommons.org/licenses/by-nc/4.0/

PES	Primary Energy Savings
Q	thermal energy, W, kW
r	discount rate
RAI	Relative Avoided Irreversibility
S	entropy, kJ/K
s	specific entropy, J/kgK
SV	yearly savings, €/year
SPT	Simple Payback Time
T	temperature, K
t	time, h
U	heat transfer coefficient, W/m^2K
Z	initial investment costs, €

Greek symbols

β	temperature coefficient, %/K
η	efficiency
ζ	exergy efficiency

Subscripts

b	boiler
CD	conduction
CV	convection
d	destruction
DHW	domestic hot water
e	environment
eg	electric grid
eng	engine
el	electrical
f	fluid, fuel
g	glass cover
HX	heat exchanger
in	inlet
irr	irradiation
k	k^{th} component
out	outlet
p	product
pv	photovoltaic
q	quality
SH	space heating
sol	solar energy
sys	system
TES	thermal energy storage
th	thermal
0	reference

1. Introduction

The building sector is the largest energy end-use sector in the European Union (EU) with a share of 41% [1]. To reduce final energy use and greenhouse gas emissions in the building sector, the energy efficiency measures for buildings have been under strong focus in research and in the content of the EU directives, such as the Energy Performance of Building Directive [2]. The EU has also set the energy efficiency targets for 2020 and 2030 by aiming to reduce energy consumption and emissions by 20% by the year 2020 and by at least 32.5% by the year 2030 compared to the 1990 level as a baseline [3]. However, despite the great energy-saving potential of the building sector, gaining the savings has proven challenging [4]. The EU Building Factsheets [4] present a

breakdown of the residential buildings by the construction year, which show that the European building stock has a significant share of older buildings constructed before 1990. Due to this, the renovating and retrofitting measurements are required to implement to already existing buildings to gain the energy-saving potential of the building sector. These measures should not only be passive measures, such as building envelope enhancement [5], but also active measures to have decentralized high efficient solutions for electricity, space heating and domestic hot water (DHW) production in buildings. The active measures should aim to have 100% renewable energy production in the building sector, which is possible with the hybrid renewable energy systems combining different energy sources, such as biomass and solar energy [6].

The key solution for the active measures to accelerate the decarbonisation of the building sector is micro combined heat and power (micro-CHP), or co-generation, systems. Micro-CHP refers to the units that produce decentralized heat and power simultaneously from a single fuel source at high efficiency. Typically, these units operate in buildings or small communities to produce energy for on-site use. The micro-CHP units typically have an electrical power of up to 15 kW [7]. However, according to the definition of the EU in the energy efficiency directive [8], micro-cogeneration refers to units with electrical power below 50 kW.

The micro-CHP system can be powered by different prime movers, such as an internal and external combustion engine or non-combustion based prime mover. Such prime movers are internal combustion engine (ICE), organic Rankine cycle (ORC), fuel cells and Stirling engine. A photovoltaic-thermal (PVT) collector is a non-combustion based cogeneration unit that converts solar energy into heat and electricity simultaneously from the same installed area. The photovoltaic (PV) panel produces electricity which generates waste heat at the same time. In the PVT collector, the PV panel has a cooling circuit underneath the panel, and the waste heat is recovered to the coolant flow to produce thermal energy. This leads to the simultaneous production of heat and power at high efficiency. However, due to the fluctuating nature of solar energy availability, the PVT collector cogenerates energy in an uncontrolled manner. On the other hand, a biomass-fuelled Stirling engine micro-CHP is the external combustion based cogeneration unit that has high fuel flexibility and produces, in a controlled manner, heat and power, simultaneously. The Stirling engine can be fuelled by renewable energy, such as biomass and solar energy. The performance of the biomass and solar energy-fuelled Stirling engines were compared by Ferreira et al. [9]. They concluded that the biomass-fuelled Stirling engine provided 87.5% more power output than the solar fuelled, had 52% lower levelized costs of electricity production and had controlled energy output.

A hybrid renewable energy system (HRES) is a second key solution for the active measures. The HRES refers to the generation of multiple energy products from the integration of two or more renewable energy sources with or without conventional energy sources and storage [10]. These systems are especially appropriate for small- and micro-scale distributed generation applications [11]. The hybridization of the solar and engine-based cogeneration units enables the use of cost-free, clean and fluctuating solar energy, and as a base-load the controllable but paid fuel energy, such as biomass. Additionally, the energy storage can be used to facilitate the energy management between the production and highly varying energy demand of a building. The hybridization enables highly efficient energy generation, increased reliability and flexibility, support for fluctuating solar energy source and the reduction in costs, primary energy use and CO_2 emissions.

Numerous studies of the domestic HRES performance with different configurations of micro-CHP and solar technologies have been conducted in the literature. The ICE based micro-CHP unit was coupled with photovoltaic (PV) panels and solar thermal collectors in [12–14] and the ORC based prime mover was studied in [15,16]. Kotowicz and Uchman studied a domestic HRES combining a natural gas-fuelled Stirling engine based micro-CHP with PV panels and electrical energy storage [17]. Aunón-Hidalgo et al. [18] presented an experimental study of a grid-connected HRES consisting of a natural gas-fuelled Stirling engine micro-CHP combined with photovoltaic panels and solar thermal collectors for a domestic environment. The energy management between the system and the domestic user was facilitated by the electrical and thermal energy storages. They conducted an energy performance and CO_2 emissions assessment of the system. Their results showed that the system was able to cover 75.6% of the total energy demand and reached 36.2% reduction in CO_2 emissions. They concluded that biogas or biomass should be used as a micro-CHP fuel instead of natural gas to achieve zero CO_2 emissions. A review on the domestic HRES based on cogeneration and solar support was presented in [19]. However, a research gap was indicated and there are no studies on a domestic HRES which combines the biomass-fuelled Stirling engine micro-CHP with the PVT collectors.

The assessment of the HRES can be extended to exergy and exergo-economic performance. The latter is used to define the specific costs of energy products from the system with multiple products and the costs flows associated with exergy flows in the system. The exergo-economic method is useful when the considered system

has multiple inputs and outputs with different exergies. Mouaky and Rachek [20] conducted a dynamic energy, exergy and exergo-economic assessment of a novel HRES driven by biomass and solar energy. The system was designed to be a polygeneration unit that, in addition to electricity cooling, heating and DHW, produced freshwater for a rural community of 40 residential buildings. Their results indicated that the system was able to cover fully the community's requirements except for cooling. The annual exergo-economic costs of the produced electricity DHW and space heating were 0.239 €/kWh, 0.043 €/kWh and 0.035 €/kWh, respectively. However, they concluded that the specific costs were competitive for remote communities but a significant reduction in the cost should be achieved to facilitate the implementation of such systems. Another dynamic exergy and exergo-economic analysis of a renewable solar-biomass HRES for polygeneration was studied by Calise et al. [21]. The system consisted of parabolic trough photovoltaic-thermal (cPVT) collectors, an absorption chiller, a biomass heater and a desalination unit. Based on their results, the cPVT collectors caused the highest exergy destruction followed by the biomass boiler in the system. The exergo-economic results revealed a high fluctuation over the year in the exergo-economic costs of the different products. Wang et al. [22] conducted an exergo-economic analysis and optimization of the HRES based on cogeneration units. The system consisted of cPVT collectors with a natural gas fired internal combustion engine (ICE) micro-CHP unit for a hotel building application to produce cooling, heating, DHW and electricity. The exergo-economic analysis was based on the energy level method. This method allows allocating the higher specific cost for the energy product with the higher energy level, such as electricity should be more expensive than low grade heat.

Within the given framework, this study aims to contribute to the existing literature through the dynamic energy, exergy and exergo-economic analysis of the cogeneration based HRES under different European climate and economic conditions to satisfy residential building energy demand. The novel HRES configuration includes PVT collectors combined with the biomass fuelled Stirling engine micro-CHP unit and thermal energy storage to facilitate the decarbonisation of the building sector.

The paper is structured as follows. In the second section, the detailed system description is provided with a modelling approach, building energy demand profiles and weather data. Additionally, the exergy and exergo-economic models are introduced with the performance indicators. In the third section, the results of the exergy and exergo-economic analysis are presented and discussed. Next, the comparative results of the HRES to the reference systems are presented and discussed. Finally, the main conclusion is drawn in the fourth section.

2. Methodology

2.1. System description

In the considered hybrid renewable energy system (HRES), the water-cooled flat plate PVT collectors are integrated with the biomass-fuelled micro-CHP system and thermal energy storage (TES). The system layout with the energy and mass flows is presented in Fig. 1. The HRES is used to produce domestic hot water, space heating and electricity for a residential building use. The cooling demand is not considered in this study. The biomass-fuelled micro-CHP is a critical component of the HRES to satisfy, especially, the thermal energy demand and the PVT collectors are used as a support to reduce costly biomass use and CO_2 emissions. The same system configuration of the HRES is applied in each location to investigate how the utilization rates of the energy production units (the micro-CHP and PVT) vary under different climates and how they impact on the exergo-economic costs of the system. The system configuration is valid in each location because the winter conditions require the controllable energy production for the significant space heating and DHW demand but there is good solar availability in each location. The annual space heating demands are presented in Fig.3 and the annual solar availability and ambient temperatures in Fig. 7.

The capacity of the micro-CHP was selected based on the market available domestic biomass-fuelled micro-CHP technology called ÖkoFen Pellematic Condens_e powered by a Stirling engine. The unit has a nominal electrical power of 1 kW and thermal power of 12 kW. This micro-CHP unit has been experimentally tested in the laboratory of INSA Strasbourg ICUBE in France and the aim of this study is to demonstrate the use of the unit in the existing residential sector. The ÖkoFen micro-CHP unit is fed by air (flow 1) and wood pellets (flow 2) to produce electricity (flow 3) and hot water (flow 4) as energy products. The coolant mass flow between the unit and TES is fixed to be 0.2 kg/s. The micro-CHP follows the heat-driven ON/OFF control strategy to satisfy the temperature levels of the thermal storage. The start-up and shut-down dynamics of the unit are neglected in this study. Additionally, the unit has internal control and is shut down if the coolant temperature reaches 75 °C.

The field of water-cooled flat plate PVT collectors is used to convert available solar radiation into heat (flow 11) and electricity (flow 12). The field consists of 9 collectors in a matrix of 3x3 to reach the higher outlet temperature from the field to the TES and to cover assumed available roof area of a typical residential building. The reference electrical efficiency of the collectors is 18.7%, and the coolant mass flow is 100 kg/h per row of the collectors. A differential temperature controller is used to control the coolant mass flow between the TES and PVT collectors. The controller compares the outlet temperature of the PVT to the temperature of the bottom of the thermal storage. The coolant mass flow is stopped or started gradually if the temperature difference is smaller or greater than 5 K to avoid cooling the storage.

The stratified 2 m^2 multi-port sensible heat storage is used to store the produced thermal energy from the micro-CHP and PVT collectors, simultaneously. Water is used as a storage medium. The volume of the storage was selected to be large to supply space heating and DHW, to enable more continues running of the micro-CHP and to store heat from two sources, simultaneously. The micro-CHP unit charges the TES to the top of the tank, and the return connection to the unit (flow 5) is at the bottom of the tank. The TES has an internal heat exchanger at the lower part of the tank to recover the heat from the PVT field. Both return connections are located at the bottom of the tank. The TES supplies heat for space heating (flow 8) of the reference building, and it has an internal heat exchanger to produce domestic hot water at 55 °C (flow 6).

The electricity flow from the micro-CHP (flow 3) and the PVT field (flow 12) are used to satisfy the power balance between the production and the electricity demand of the building presented in Fig. 5. The surplus electricity is fed to the electric grid.

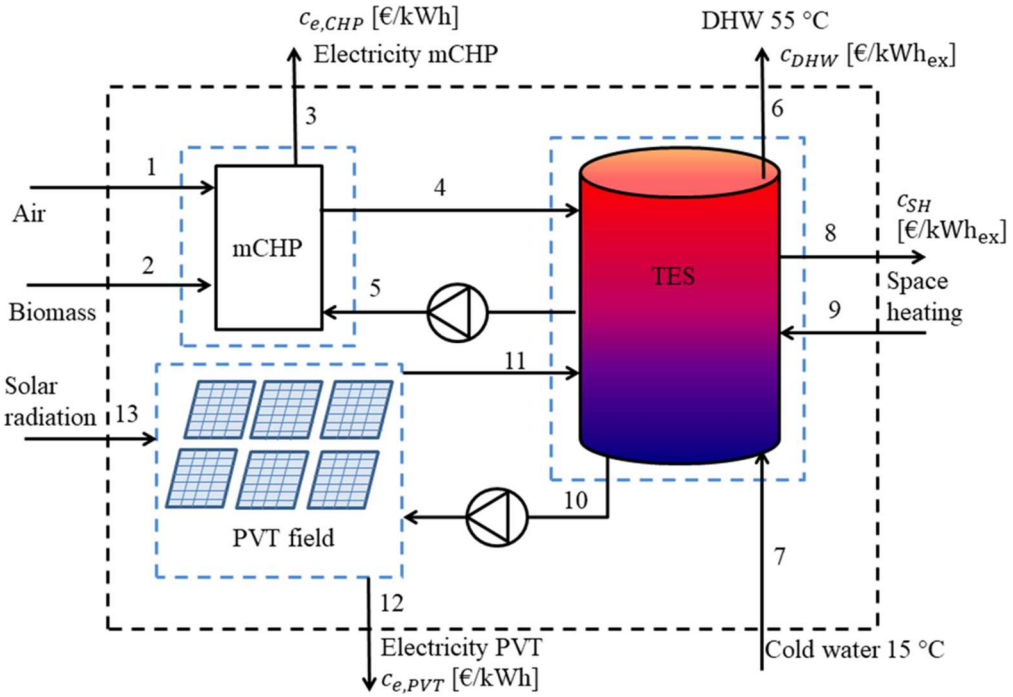

Fig. 1. The system layout and control volumes of the hybrid renewable energy system.

The main characteristics of the described HRES are presented in Table 1.

Table 1. The main characteristics of the hybrid renewable energy system

Component	Parameter	Value	Unit
Micro-CHP	Thermal power	12	kW
	Electrical power	1	kW
	Fuel	Wood pellets	
PVT	Area single	2	m^2
	Ref. electrical efficiency	18.7	%

	PVT in series	3	-
	PVT in rows	3	-
TES	Volume	2	m^2
	Insulation	0.3	W/m^2K

2.2. Simulation models

A dynamic simulation model of the described HRES was built into Matlab/Simulink environment to analyze its yearly exergetic and exergo-economic performance.

The open-source CARNOT-Toolbox [23] was used to model the stratified multi-port thermal energy storage, pipe connections, thermostatic flow mixers for heat supply, valves and pumps. The validated tank model called "Storage_Type_5" was used in which the storage volume is divided into 6 nodes to present the stratification. For each node, the energy balance is calculated to find the current temperature of each node. The detailed tank model is presented in [24]. The thermostatic flow mixers were used to control the required heat supply temperatures of 40°C for space heating and 55°C for DHW.

In the authors' previous work [25], a single water-cooled flat plate PVT collector with glazing and sheet-and-tube heat exchanger was modelled into Matlab/Simulink and extended to present a field of the PVT collectors. The model considers the main heat transfer mechanisms between each PVT layer, such as the glass cover, PV module, absorber and coolant fluid. The electricity conversion efficiency of the PVT collector depends linearly on the PV module temperature T_{pv}, the temperature coefficient β_{PV} and the efficiency η_{STC} at standard conditions T_{ref}. The key governing equations of the PVT collector in terms of thermal and electrical energy are following:

$$m_g \times c_{p,g} \times dT_g/dt = Q_{g,sol} + Q_{g-e,CV} + Q_{g-sky,RD} + Q_{g-pv,CV} + Q_{g-pv,RD} \quad (1)$$

$$m_{pv} \times c_{p,pv} \times dT_{pv}/dt = Q_{pv,s} + Q_{pv-g,CV} + Q_{pv-g,RD} + Q_{pv-f,CV} - E \quad (2)$$

$$m_f \times c_{p,f} \times dT_f/dt = Q_{f-pv,CV} + Q_f \quad (3)$$

$$\eta_{el(T)} = \eta_{STC} \times \left[1 - \beta_{PV} \times \left(T_{pv} - T_{ref}\right)\right] \quad (4)$$

The detailed description of the used model and the validation can be found in [25].

The considered HRES includes the ÖkoFEN Pellematic Condens_e unit which is a biomass-fuelled Stirling engine micro-CHP system and has been experimentally tested in the laboratory of INSA Strasbourg ICUBE in France. The mathematical model of the system is based on Annex 42 [26] modelling approach of the external combustion engine and the following energy balance governing equations are implemented to Simulink to model the heat transfer to the coolant fluid [27]:

$$MC_{eng}\, dT_{eng}/dt = UA_{HX} \times \left(T_{w,out} - T_{eng}\right) + UA_{loss} \times \left(T_{env} - T_{eng}\right) + q_{gen} \quad (5)$$

$$MC_w \times dT_{w,out}/dt = \dot{m}_w \times c_{p,w} \times \left(T_{w,in} - T_{w,out}\right) + UA_{HX} \times \left(T_{eng} - T_{w,out}\right) \quad (6)$$

The previously collected experimental data of the considered micro-CHP was used to validate and identify the thermal capacity of the engine MC_{eng} and cooling water MC_w, and the engine specific heat transfer coefficients UA_{HX} and UA_{loss}. The identification was performed with Simulink Parameter Estimator Tool.

The recovered heat from the micro-CHP control volume Q_{CHP} is calculated from the cooling water mass flow rate m_w and temperature difference between the inlet and outlet of the flow [28].

$$Q_{CHP} = \dot{m}_w \times c_w \times \left(T_{w,in} - T_{w,out}\right) \quad (7)$$

2.3. Building energy demand

The considered HRES is installed in a single or multi-family house in different locations. As a reference building, a single-family house presented in Fig. 2 was selected and simulated in the IDA ICE building simulation tool [29]. The building U-values were defined based on the building factsheets of the European Union [4], which represent the building stock characteristics in different European countries. Based on this average building performance data, the defined reference building was simulated under different climate conditions with the country-specific U-values of the building shell. The hourly heating demand profiles were obtained from the simulation in the different European locations and used in the exergo-economic analysis. The selected locations were Tampere, Finland; Strasbourg, France and Barcelona, Spain. The geometry of the reference building and building performance parameters in the different locations are presented in Table 2.

Fig. 2. The reference building used in the building simulation.

Table 2. The main characteristics of the reference buildings and the climate classifications in each location [4].

Parameter	Building geometry	U-value [W/m^{2}K]		
		Finland	France	Spain
Windows	19 m^2	1.76	2.83	4.16
Walls	111 m^2	0.34	0.97	1.32
Floor	150 m^2	0.32	0.89	1.03
Roof	143 m^2	0.23	0.83	1.45
Windows to wall ratio	0.17			
Climate classification		Subarctic	Semi-continental	Dry-summer subtropical

The annual results of the hourly thermal load in three locations are presented in Fig. 3. This Figure shows that space heating is required during the whole year in the northernmost location of Tampere resulting in the annual demand of 152 kWh/m^2. In Strasbourg, the annual demand is 160 kWh/m^2. The milder climate conditions of Strasbourg did not reduce the heating demand compared to Tampere, because of the higher U-values of the building envelope. However, during the summer period the heating demand was slightly lower in Strasbourg than in Tampere as shown in Fig. 3. In Barcelona, the annual heating demand was significantly lower than in Tampere and Strasbourg due to the warmer climate resulting in 86 kWh/m^2. In Barcelona, there was no space heating demand during July, August and September.

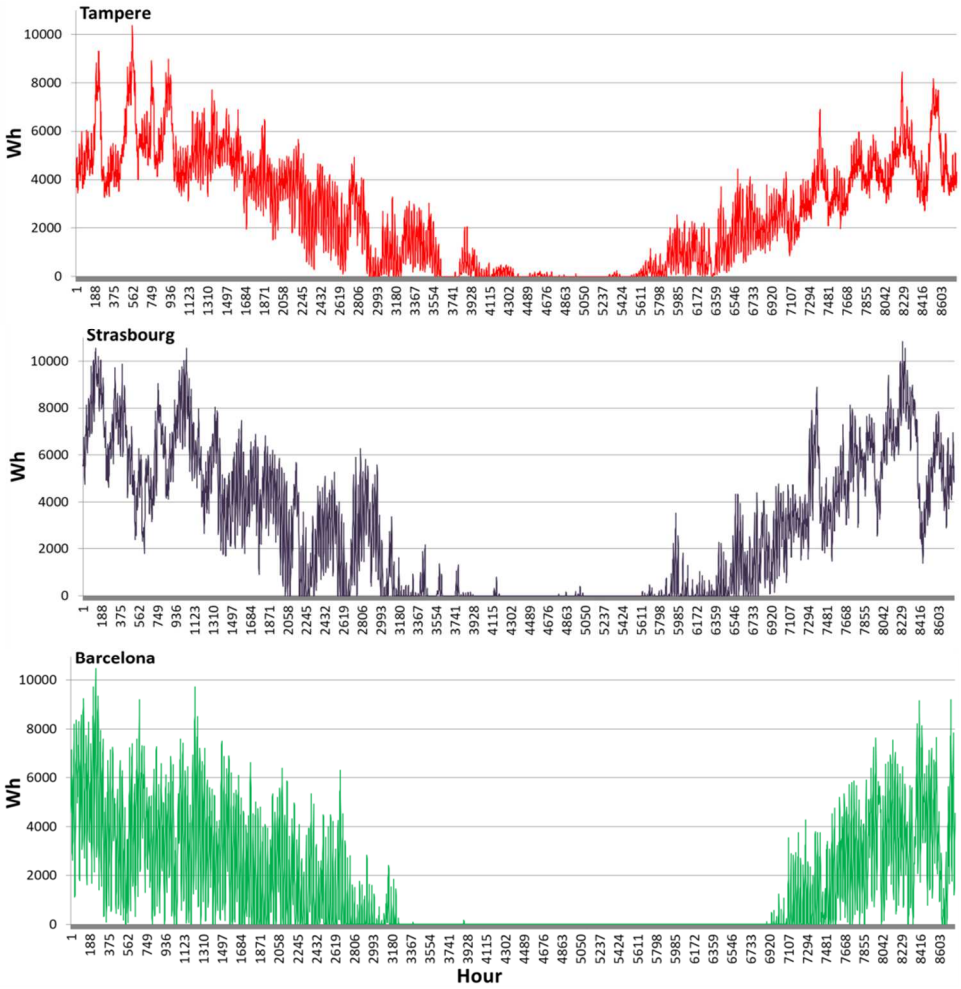

Fig. 3. The annual results of the hourly thermal load in each location.

In addition to space heating, the HRES is used to produce domestic hot water (DHW). The reference building is assumed to include 4 inhabitants with 250 l/day average consumption. The hourly DHW demand profile based on probability distribution was generated using the DHW-calc tool developed for IEA-SHC Task 26 at the University of Kassel in Germany [30,31]. The different parameters, such as the average daily consumption, flow rates and daily, weekly and monthly weighting of the consumption, were defined to generate a realistic DHW demand profile suitable for each location. An example of the demand profile is presented in Fig. 4.

In the system simulations, the temperature of the cold water entering the system from the mains was assumed to be at 15°C during the year in each location and the water was heated up to 55 °C.

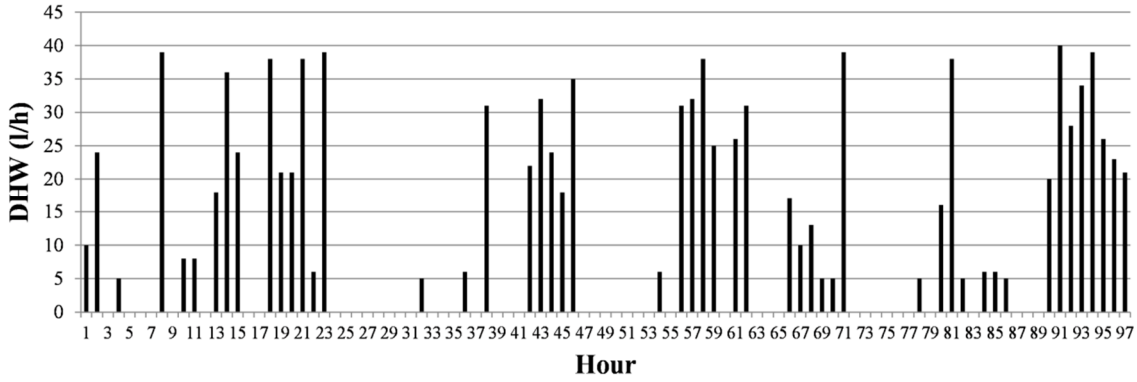

Fig. 4. The hourly DHW demand profile generated by the DHW-calc tool.

The electricity demand profile was assumed to be the same in each location. The normalized standard electricity demand profiles for residential buildings generated by the German Association of Energy and Water Industries, BDEW (Bundesverband der Energie- und Wasserwirtschaft) [32] are used to simulate electricity demand every 15 min for certain yearly consumption. The profile takes into account electrical appliances excluding special applications, such as heat pumps and electrical storage heaters. The used electricity profile includes three different periods of the year: winter, summer and transition. Additionally, three different types of the day are presented: workday, Saturday and Sunday/holiday. Figure 5 shows the sample of the profile during a summer period. In the analysis, the yearly consumption of 6000 kWh was assumed for a single-family house in each location.

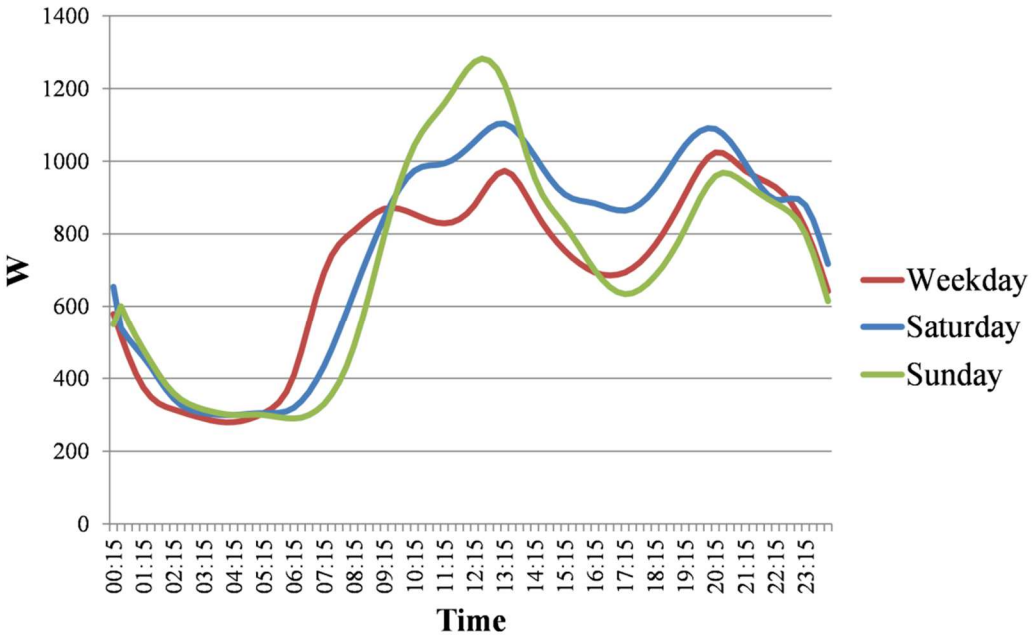

Fig. 5. The electricity profile for a day (weekday, Saturday and Sunday).

2.4. Meteorological data

The proposed HRES is studied under three different European climate conditions because the energy yield of the PVT collectors depends strongly on the weather parameters, such as solar radiation, wind speed and ambient temperature. The performance of the PVT collectors has a direct impact on the available solar support in the hybrid energy system and on the fuel costs reduction.

The selected locations are Tampere, Finland; Strasbourg, France and Barcelona, Spain. According to the Köppen climate classification presented in Fig. 6, Tampere represents Northern Europe with a subarctic climate border. This means that the ambient temperature reaches above 10 °C only 3 months in a year [25]. Strasbourg represents Central Europe, and according to the classification, it has a semi-continental climate with cool winters and relatively sunny summers. The Mediterranean location Barcelona represents South of Europe, and according to the classification, it has a dry-summer subtropical climate. This means hot and dry summer with a cooler and wetter wintertime.

Fig. 6. The Köppen-Geiger Climate Classification map [33].

Figure 7 shows the global solar irradiation and ambient temperature over year in each location. The presented hourly weather data is obtained from the IDA ICE building simulation software and is based on the ASHRAE IWEC (International Weather for Energy Calculation) database [34]. In this database, the weather files for different locations are derived from the collected hourly weather data for up to 18 years [35]. These "typical" weather files for different locations smooth the yearly variation of the weather conditions.

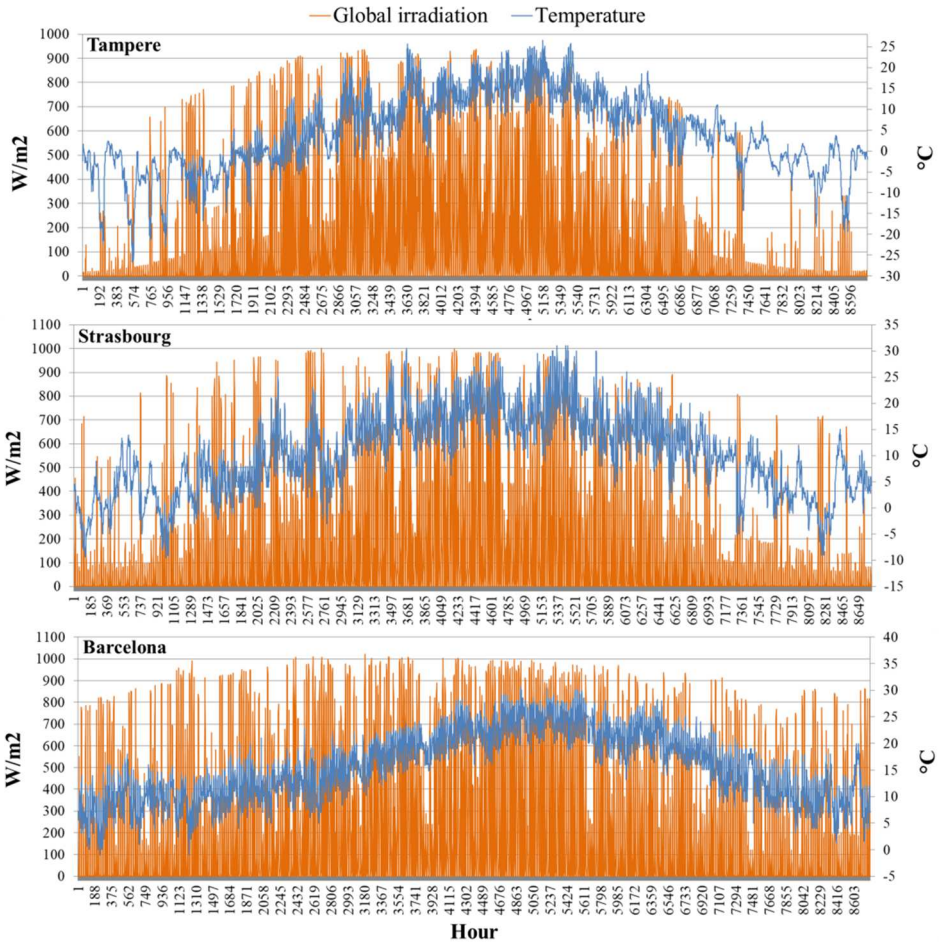

Fig. 7. The hourly solar radiation and ambient temperature based on the historical data in each location [34].

The monthly average ambient temperatures are presented in Table 3. This data is used in the exergy and exergo-economic analysis as monthly reference temperatures in order to take into account the impact of the location to thermal exergy production.

Table 3. The monthly average temperatures in each location [34].

Month	Tampere, average temperature [°C]	Strasbourg, average temperature [°C]	Barcelona, average temperature [°C]
January	-6.3	2.3	8.2
February	-6.6	2.1	9.4
March	-2.5	6.0	11.2
April	3.3	9.9	13.2
May	9.6	14.7	17.1
June	13.5	17.4	21
July	16.6	18.9	23.6
August	15.1	19.0	24
September	9.2	14.7	21.5
October	4.6	10.5	17.2
November	-1.2	4.8	12
December	-4.2	2.7	9.7

338

339 *2.5. Exergy analysis*

340 The exergy analysis is based on the Second Law of Thermodynamics and it quantifies the quality of the input
341 and output in the energy conversion process. It complements the First Law based energy analysis by counting
342 how well the quality of the fuel energy is maintained in the conversion process while energy analysis quantifies
343 only the amount of energy produced and lost in the process. Through the energy conversion process, exergy is
344 always destroyed but energy changes its form and is never destroyed. The exergy analysis helps to reveal better
345 inefficiencies in the conversion process. The quality of energy is counted as a work potential to the specific
346 environment or reference temperature. Typically, this state is the environmental conditions of the energy
347 conversion device. The selection of the reference temperature defines the exergy of the system and it should be
348 selected carefully. In this study, the monthly exergy and exergo-economic analysis is conducted under different
349 climate conditions and the monthly average ambient temperatures in Table 3 are used as reference temperatures.
350 The exergy balance of the cogeneration is generally presented as follows:

$$\sum Ex_{in} - \sum (Ex_{el} + Ex_{th}) = \sum Ex_d \tag{8}$$

351 where Ex_d is the exergy destruction, Ex_{in} is the exergy content of the used fuel, and Ex_{el} and Ex_{th} represent
352 the electrical and thermal exergy products, respectively. The exergy efficiency is calculated by dividing the sum
353 of the exergy products by fuel exergy.
354 The considered system receives the fuel exergy from biomass and solar radiation. The PVT field absorbs
355 exergy from solar radiation which is not seen as pure exergy but a following conversion conversation coefficient
356 is used to calculate incoming exergy [36]:

$$Ex_{in,PVT} = A_c \times G_{irr} \times (1 - 4/3 \times T_0/T_{sol} + 1/3 \times (T_0/T_{sol})^4) \tag{9}$$

357 In Equation (9) T_0 is the monthly reference temperature in Kelvin and T_{sol} is the solar temperature (5777 K).
358 The fuel exergy of biomass is defined as follows [37]:

$$Ex_{in,CHP} = f_{q,biomass} \times \dot{m}_f \times LHV_{biomass} \tag{10}$$

359 where $f_{q,biomass}$ is a quality factor of wood pellets and $LHV_{biomass}$ is the lower heating value of 4900 Wh/kg. In
360 this study, the quality factor of 1.13 is used for wood pellets [38].
361 As an energy product, electricity is seen as pure exergy which can be totally transformed into work.
362 However, the exergy content of thermal energy flow from the micro-CHP, PVT field and thermal energy storage
363 depends on the specific enthalpy (h) and entropy (s) of the water flow at the inlet and outlet of the certain
364 component. The specific enthalpy and entropy of the certain flow depends on the temperature at which the flow
365 is made available. The thermal exergy of water flows in the system is presented as follows [37,39]:

$$Ex_{th} = \dot{m} \times [h_{out} - h_{in} - T_0 \times (s_{out} - s_{in})] = \dot{m} \times c_{p,f} \times [(T_{out} - T_{in}) - T_0 \times ln\, T_{out}/T_{in}] \tag{11}$$

366 where ṁ is the mass flow rate, $c_{p,f}$ is the fluid specific heat.

367 *2.6. Performance indicators*

368 The considered HRES has highly dynamic behaviour due to dependence on the fluctuating solar radiation
369 and energy demand. Due to this cumulative energy and exergy flows are used to calculate the performance
370 indicators over defined periods:

$$Ex_j = \int_{period} \dot{Ex}_j \, dt \tag{12}$$

371 The period is defined to be a month to see the difference in the performance indicators during a year.
372 The exergy efficiency of the whole HRES is presented as follows:
373

$$\zeta_{overall} = \frac{(Ex_8 - Ex_9) + (Ex_6 - Ex_7) + Ex_3 + Ex_{12}}{Ex_{in,CHP} + Ex_{in,PVT}} \quad (13)$$

where the exergy products are space heating, domestic hot water and electricity produced by the PVT field and micro-CHP unit.

The operation of the considered hybrid energy system including cogeneration units can be compared to separated production of heat and electricity. The defined reference system for separated energy production includes the electric grid based on the centralized nuclear power plant and a natural gas-fuelled boiler. The energy based comparison indicator is Primary Energy Savings (PES) [37]:

$$PES = \left(1 - \frac{1}{\frac{\eta_{el}}{\eta_{eg}} + \frac{\eta_{th}}{\eta_b}}\right) \times 100 \quad (14)$$

The PES indicator shows the saved primary energy when cogeneration is used instead of the separated energy production. However, this indicator qualifies electricity and heat to be the same value but, in terms of exergy, heat has lower quality than electricity. This leads to a fact that it is not reasonable to directly compare the different energy products of the system. Thus, an exergy-based comparison indicator called Relative Avoided Irreversibility (RAI) [37,40] is used and presented as follows:

$$RAI = \left(1 - \frac{Ir_{CHP}}{Ir_{eg} + Ir_b}\right) \times 100 \quad (15)$$

$$Ir = (1 - \zeta) \times Ex_{in} \quad (16)$$

where Ir is the generated exergy irreversibility or destruction of the certain energy conversion process.

2.7. Economic and Exergo-economic assessment based on energy level and varying reference temperatures

In this study, the considered HRES is economically assessed by the economic indicators called Simple Payback-Time (SPT) and Net Present Value (NPV) and by an exergo-economic analysis which specifies the costs of the energy products from the HRES.

2.7.1. Economic indicators

The SPT gives a rough estimation of the economic viability of the considered system by dividing the initial investment costs (Z_{sys}) by all counted revenues/savings that the system can generate during yearly operation. However, it does not take into account the time value of cost which results in the rough estimation of the payback-time in years. This indicator is calculated as follows [41]:

$$SPT = Z_{sys}/SV_{sys,year} \quad (17)$$

where $SV_{sys,year}$ is the yearly savings compared to a reference system and calculated as follows [41].

$$SV_{sys,year} = \left(E_{el,load} \times c_{el,fromGrid} + \frac{\left(Q_{th,SH} + Q_{th,DHW}\right) \times c_{NG}}{LHV_{NG}\eta_b}\right)_{RS} - \left(m_{biomass} \times c_{biomass} + E_{el,fromGrid} \times c_{el,fromGrid} - E_{el,toGrid} \times c_{el,toGrid} + OM_{CHP}\right)_{HRES} \quad (18)$$

where RS indicates the reference system and HRES the considered hybrid system.

Another useful economic indicator to evaluate the economic viability is the NPV, which takes into account time by discounting future savings to the present value over the lifetime of the HRES. A positive NPV indicates

economically acceptable investment and a negative indicates unviable investment under considered circumstances.

$$NPV = -Z_{sys} + \sum_{n} \left(a \times SV_{sys,year}\right) \tag{19}$$

$$\mathrm{a} = 1/(1+r)^{n} \tag{20}$$

where a is the annuity factor, r is the discount rate and n is the lifetime of the system.

2.7.2. Exergo-economic analysis

The exergo-economic analysis combines exergy with economic analysis and is used to allocate the initial investment and operating and maintenance (O&M) costs for the energy products of the. In this study, the Specific Exergy Costing (SPECO) approach proposed by Lazzaretto and Tsatsaronis [42] is used. Based on that method, a cost value can be assigned to exergy unit of each energy flow in Fig. 1 coming and leaving a certain system component. The exergy costing method reveals the prices for the produced electricity and heat that should be returned or saved to cover the initial investment and O&M costs of the HRES. According to the SPECO, the exergy cost balance equation of the k^{th} component in steady operating conditions can be written as follows:

$$\dot{\mathrm{C}} = \mathrm{c} \times \dot{\mathrm{E}}\mathrm{x} \tag{21}$$

$$\sum_{\text{fuel}} \left(\mathrm{c_f} \times \dot{\mathrm{E}}\mathrm{x_f}\right)_{\mathrm{k}} + \dot{\mathrm{Z}}_{\mathrm{k}} = \sum_{\text{product}} \left(\mathrm{c_p} \times \dot{\mathrm{E}}\mathrm{x_p}\right)_{\mathrm{k}} \tag{22}$$

where $\dot{\mathrm{C}}$ is exergy cost rate in €, c is the specific cost of exergy in €/kWh$_{ex}$ and $\dot{\mathrm{E}}\mathrm{x}$ is the exergy rate in kW. Due to the fluctuating nature of solar energy production, the cumulative exergy flows over defined period based on Eq. (12) are taken into account and the exergy rates in Eq. (22) are replaced by the cumulative values. In Eq. (22), $\dot{Z}$ represents non-exergetic costs including initial investment costs and O&M costs of the component with the Capital Recovery Factor (CRF). The cumulative non-exergetic costs are presented as follows:

$$\tilde{Z}_k = I_k \times CRF \times t_{period}/8760 + OM_k = I_k \times \frac{i(1+i)^n}{(1+i)^n - 1} \times t_{period}/8760 + OM_k \tag{23}$$

where t_{period} is the length of considered period, i is the interest rate, n is the lifetime of the component and OM is the O&M costs over the considered period. It is assumed to be 1.5% of the levelized investment cost of the period for the micro-CHP unit.

The considered HRES has multiple outputs and it includes cogeneration components that have multiple products. Due to this, auxiliary costing equations are required to define the specific cost of the multiple products. Additionally, the energy levels of different energy products are taken into account in the costing method according to [43]. The energy level reveals the quality of the energy flow and its ability to work to the reference temperature [43]. By considering the energy level, the specific cost of any flow is directly proportional to its energy level and gives the higher price for the higher quality flow. This leads to more realistic evaluation of the exergo-economic performance of different energy product.

The energy level of electricity is 1 but the level of heat depends on the following formula [43]:

$$EL = 1 - T_0\, \Delta S/\Delta H \tag{24}$$

where T_0, ΔS and ΔH are the reference temperature, entropy change and enthalpy change, respectively.

In addition to the energy levels, the location and period specific reference temperatures in Table 3 were taken into account in the monthly exergo-economic analysis in order to have a fair comparison between different locations of the HRES.

Next, the exergo-economic model of the HRES in Fig. 1 is presented. The model includes a number of cost balances and n-1 auxiliary costing equations for three main components: micro-CHP, PVT field and thermal energy storage. Table 4 presents the economic parameters used in the exergo-economic analysis. The initial investment costs are presented without the country specific Value Added Tax (VAT) which is taken into account in the calculations. The VAT is 24% for Finland, 20% for France and 21% for Spain.

Table 4. The economic parameters of the exergo-economic analysis.

Parameter	Description	Value	Unit	Ref.
I_{CHP}	Initial investment costs of micro-CHP	17600	€	ÖkoFEN company
OM_{CHP}	O&M costs of micro-CHP	1.5	%	
I_{PVT}	Initial investment costs of PVT	295	€/m^2	DualSun company
I_{inv}	Initial investment costs of inverters	100	€/piece	Enphase company
I_{TES}	Initial investment costs of TES	2300	€/m^3	Sailer company
c_{DHW}	Specific costs of tap water	0.00083	€/kg	[44]
$LHV_{biomass}$	Biomass lower heating value	4900	Wh/kg	
LHV_{NG}	Natural gas lower heating value	9.6	kWh/Sm^3	[41]
$\eta_{el,heater}$	Efficiency of electric heater	95	%	
η_b	Efficiency of natural gas boiler	80	%	
r	Discount rate	2	%	
N	Lifetime	25	years	

Micro-CHP

The biomass-fuelled micro-CHP unit uses air, which is free of charge, biomass and the non-exergetic cost $\tilde{Z}_{CHP}$to produce electricity (flow 3) and heat (flow 4), simultaneously. This leads to a following cost balance and auxiliary equations:

$$\dot{C}_1 + \dot{C}_2 + \tilde{Z}_{CHP} = \dot{C}_3 + \left(\dot{C}_4 - \dot{C}_5\right) \tag{25}$$

$$\dot{C}_1 = 0 \tag{26}$$

$$\dot{C}_2 = \dot{m}_{biomass} \times c_{biomass} \tag{27}$$

where $\dot{m}_{biomass}$ is the mass flow of wood pellets (kg/h) and $c_{biomass}$ is the specific cost of wood pellets in €/kg.

Based on the fuel and product rule of the SPECO [42] and on the fact that the specific costs of electricity and heat produced by the micro-CHP unit are directly proportional to their energy levels, the following auxiliary equation are written:

$$c_3/EL_3 = \ (c_4 - c_5)/EL_{4-5} \tag{28}$$

$$\frac{\dot{C}_3 \times \left(\dot{Ex}_4 - \dot{Ex}_5\right)}{\dot{Ex}_3 \times \left(\dot{C}_4 - \dot{C}_5\right)} = EL_3/EL_{4-5} \tag{29}$$

Finally, the specific costs of electricity from the micro-CHP unit are formulated as follows:

$$c_{el,CHP} = \frac{\dot{C}_2 + \tilde{Z}_{CHP}}{\left(1 + \frac{\left(\dot{Ex}_4 - \dot{Ex}_5\right) \times EL_{4-5}}{\dot{Ex}_3 \times EL_3}\right)\dot{Ex}_3} \tag{30}$$

PVT

The PVT field consumes solar energy (flow 13), which is free of charge, and the non-exergetic costs $\tilde{Z}_{PVT}$to produce electricity (flow 12) and heat (flow 11), simultaneously. This leads to a following cost balance and auxiliary equations:

$$\dot{C}_3 + \tilde{Z}_{PVT} = \dot{C}_{12} + \left(\dot{C}_{11} - \dot{C}_{10}\right) \tag{31}$$

$$\dot{C}_3 = 0 \tag{32}$$

$$c_{12}/EL_{12} = (c_{11} - c_{10})/EL_{11-10} \quad (33)$$

$$\frac{\dot{C}_{12}(\dot{Ex}_{11} - \dot{Ex}_{10})}{\dot{Ex}_{12}(\dot{C}_{11} - \dot{C}_{10})} = \frac{EL_{12}}{EL} \quad (34)$$

Finally, the specific costs of electricity from the PVT field are formulated as follows:

$$c_{el,PVT} = \frac{\tilde{Z}_{PVT}}{\left(1 + \frac{(\dot{Ex}_{11} - \dot{Ex}_{10})EL_{11-10}}{\dot{Ex}_{12}EL_{12}}\right)\dot{Ex}_{12}} \quad (35)$$

Thermal energy storage

The thermal storage receives heat "fuel" from the micro-CHP and PVT field and uses the non-exergetic costs $\tilde{Z}_{TES}$ to store and exchange the heat to feed DHW and space heating circuits when necessary. The following cost balances are written for the TES:

$$(\dot{C}_4 - \dot{C}_5) + (\dot{C}_{11} - \dot{C}_{10}) + \dot{Z}_{TES} = (\dot{C}_8 - \dot{C}_9) + (\dot{C}_6 - \dot{C}_7) \quad (36)$$

$$\dot{C}_7 = \dot{m}_7 \times c_{DHW} \quad (37)$$

$$(c_8 - c_9)/EL_{8-9} = (c_6 - c_7)/EL_{6-7} \quad (38)$$

$$\frac{(\dot{C}_8 - \dot{C}_9)(\dot{Ex}_6 - \dot{Ex}_7)}{(\dot{Ex}_8 - \dot{Ex}_9)(\dot{C}_6 - \dot{C}_7)} = \frac{EL_{8-9}}{EL_{6-7}} \quad (39)$$

where $\dot{m}_7$ is the domestic hot water demand and c_{DHW} is the specific cost of tap water in €/kg.

Hybrid renewable energy system

Finally, the specific costs of electricity ($c_{el,sys}$), domestic hot water (c_{DHW}) and space heating (c_{SH}) are calculated as follows:

$$c_{el,sys} = \frac{\dot{C}_3 + \dot{C}_{12}}{\dot{Ex}_3 + \dot{Ex}_{12}} = \frac{c_{el,CHP} \times \dot{Ex}_3 + c_{el,PVT} \times \dot{Ex}_{12}}{\dot{Ex}_3 + \dot{Ex}_{12}} \quad (40)$$

$$c_{DHW} = \dot{C}_6/\dot{Ex}_6 \quad (41)$$

$$c_{SH} = (\dot{C}_8 - \dot{C}_9)/(\dot{Ex}_8 - \dot{Ex}_9) \quad (42)$$

3. Results and discussion

The simulation tool was built into Matlab/Simulink to evaluate the exergetic and exergo-economic performance of the HRES in Fig. 1 under three different European climate conditions described in Section 2.4. The tool allows calculating exergy production, destruction and efficiency on the component and system level over a certain period. Additionally, the calculations of the exergo-economic specific costs of electricity, domestic hot water and space heating produced by the HRES can be conducted on the monthly basis.

3.1. Exergy analysis

Next, the results of the exergy analysis of the system in each location are presented and discussed. The aim of the considered HRES was to support energy production of the biomass micro-CHP with solar cogeneration in order to reduce biomass consumption and costly exergy destruction. Solar energy as a fuel has lower quality than biomass, and it is free of charge.

In Fig. 8 are presented the exergy fuel, product and destruction flows over three representative days from spring, summer and winter periods in Strasbourg.

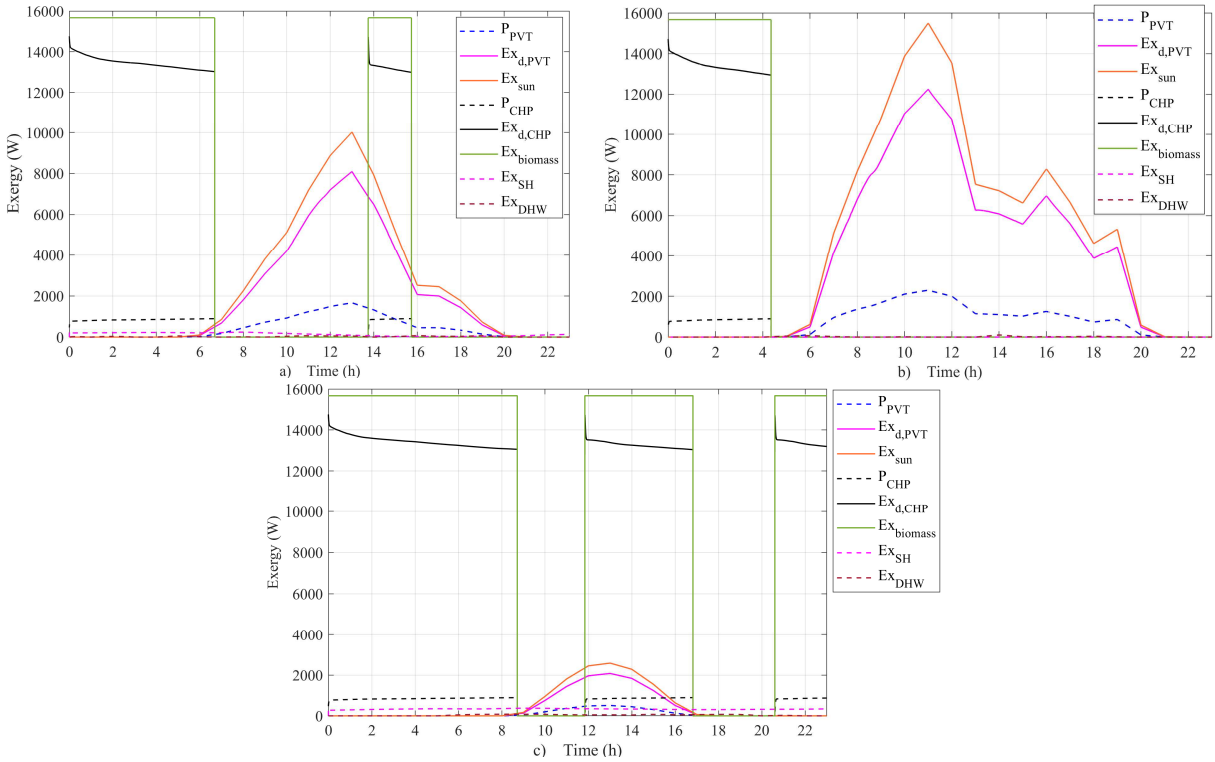

Fig. 8. The fuel, product and destruction exergy flows during three different days in Strasbourg a) in spring, b) in summer and c) in winter.

Figure 8 shows the variation of the utilized solar and biomass exergies over time. On each day, the micro-CHP run during the night hours to satisfy the space heating and to maintain the temperature of the TES. The reduced solar availability during the spring and winter day forced to use biomass exergy also during the day hours. During the winter day, the main fuel exergy came from biomass use. The exergy destruction in both micro-CHP and PVT was significantly higher compared to the exergy products that are space heating, DHW and electricity. The magnitude of the space heating and DHW exergy products was low due to the low temperature levels. The highest exergy product was the electricity produced by PVT during the spring and summer days and the electricity produced by the micro-CHP during the winter day.

The exergy analysis in Fig. 8 revealed a big difference between the magnitudes of the used fuel exergy fed to the system and the gained exergy products. The costly exergy destruction in the Stirling engine micro-CHP unit could be reduced by improving the electrical power output of the unit.

In Fig. 9 is presented the used fuel exergy in each location. The higher availability of solar radiation during the summer months increased the solar share of the total fuel exergy. However, the solar share was also increased due to decreased energy demand of the building. Figure 9 clearly shows that in the southernmost location of Barcelona, the solar share of the fuel exergy was significant also during the winter months from November to March covering at worst 26% of fuel exergy in January. At the same time, the solar share was below 10% in Strasbourg and Tampere. This trend was seen in November and December as well.

Figure 9 reveals that despite the northern location of Tampere, the solar share of the fuel exergy was close to one in Strasbourg. However, in September the solar share was only 52% while it was still 78% and 97% in Strasbourg and Barcelona, respectively.

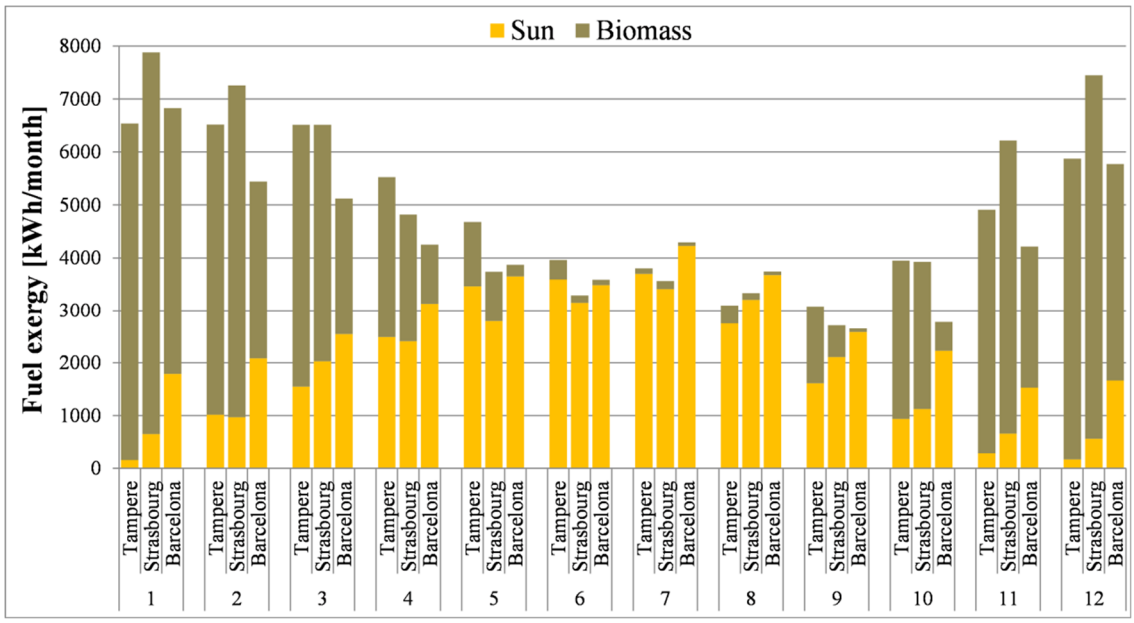

Fig. 9. The monthly fuel exergy flows in each location.

Figure 10 shows the total exergy destruction divided for each system component (PVT, micro-CHP and TES) in each location. The exergy destruction was higher during the winter months from November to March because of the high demand for low-grade heat production for space heating. During these months, the micro-CHP caused most of the destruction in the system while the PVT dominated the destruction during the summer months. The TES was used to manage thermal exergy flows in the system and counted the smallest part of the total exergy destruction. However, the exergy destruction of the TES was significantly higher during the winter months. This was caused by using high thermal exergy flow from the micro-CHP to produce a high amount of space heating which had low exergy content. On the other hand, during the summer months, while the space heating was almost zero, the low thermal exergy flow from the PVT field was used to produce domestic hot water which had high exergy content resulting in lower exergy destruction.

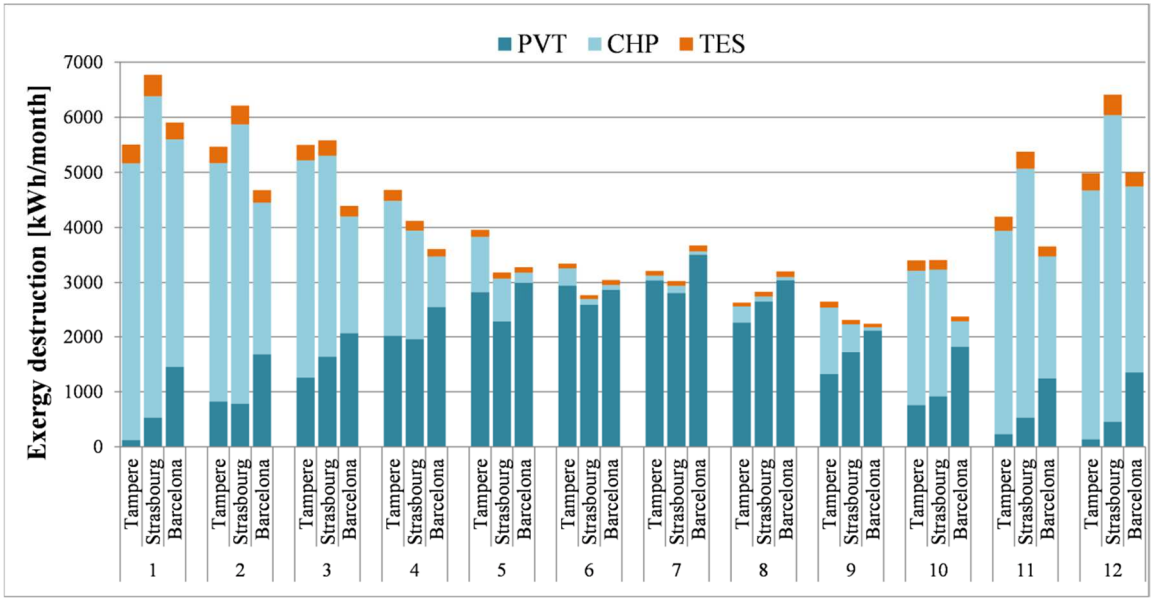

Fig. 10. The monthly exergy destruction in each location divided for each component.

The exergy products from the HRES were space heating, domestic hot water and electricity produced by the micro-CHP unit and PVT field. These exergetic products are presented on monthly basis in Fig. 11.

Figure 11 reveals that the exergy products were dominated by the electrical exergy produced by the PVT field. In the sunny location of Barcelona, the proportion of the PVT electricity was already higher than the one of the micro-CHP in January although the operation of the micro-CHP was high due to higher space heating demand. The same happened in Tampere and Strasbourg in March. This result show that the hybridization of the units increased significantly the free-fuel based electricity production capacity of the HRES. Additionally, the solar support helped to reduce biomass use and costly exergy destruction during the whole year.

In Tampere and Strasbourg, the space heating was a significant exergy product during the cooler months from November to February. However, the quality of the space heating as an exergy product depended on the reference temperature of the considered location. Due to this, the exergy of the heat products was the lowest in the warmest location of Barcelona.

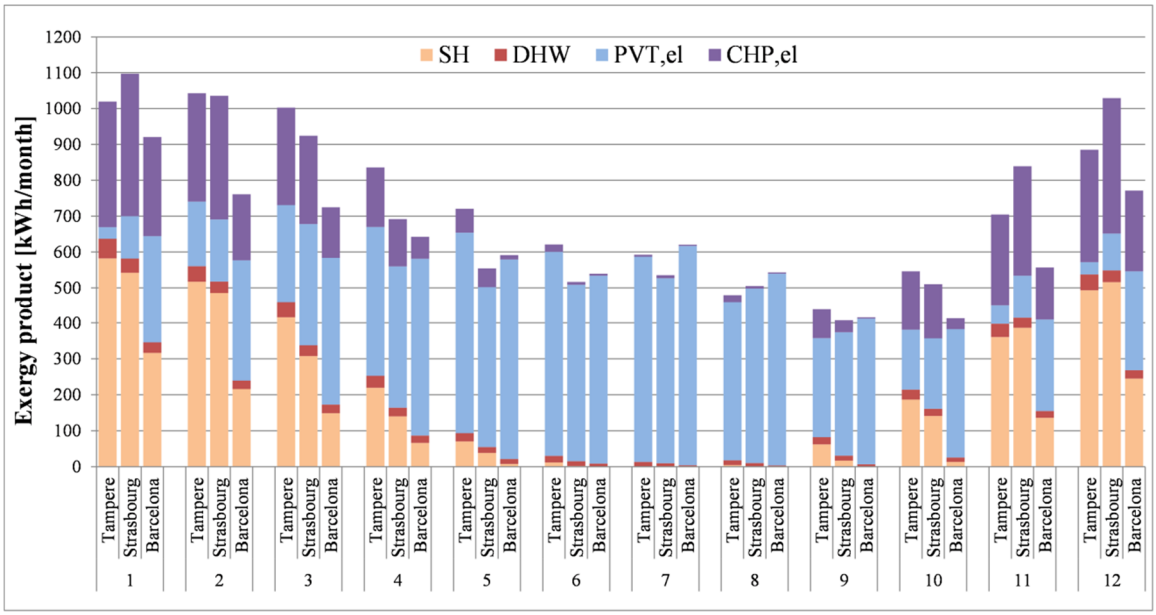

Fig. 11. The monthly exergy products from the hybrid renewable energy system in each location divided for each energy product of the system.

Figure 12 shows the monthly overall exergy efficiency of the HRES in the selected locations. The exergy efficiency varied from 13% to 16% reaching the maximum value in Tampere already in February, in Strasbourg in June and in Barcelona in September. Due to the significantly cooler monthly reference temperatures, the efficiency was the highest in Tampere during the winter months. In Strasbourg and Barcelona, the exergy efficiency increased slowly from January to June and to May, respectively, while the solar irradiation increased and heating demand decreased. In each location, the exergy efficiency decreased strongly at the end of the year due to strongly reduced solar irradiation and increased use of the micro-CHP system for space heating demand. The decrease was strongest in Strasbourg from September to October by 2% percentage points. In Tampere and Barcelona, the fall in efficiency was slower and took place from August to October and from September to November, respectively.

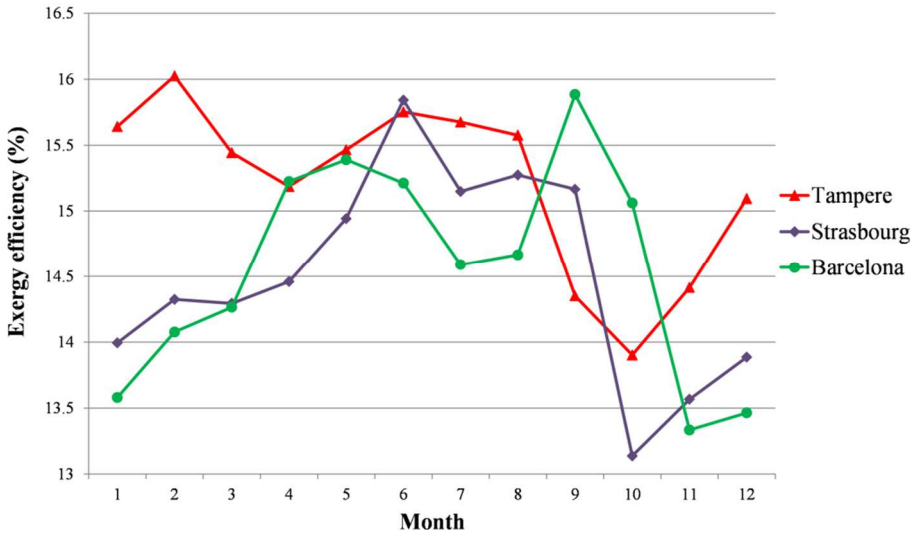

Fig. 12. The monthly exergy efficiency of the whole system in each location.

The yearly overall exergy efficiency, given by Eq. (13), was the highest in Tampere resulting in 15.3% followed by Strasbourg and Barcelona with the same result of 14.3%. The efficiency was the highest in Tampere due to the coolest monthly reference temperatures which led to the higher exergy of the heat products. This increased relatively the amount of the total exergy products compared to the other locations. Barcelona and Strasbourg resulted in the same annual overall exergy efficiency. This was possible due to the different utilization rates of the energy production units of the system. Due to the higher heating demand, the micro-CHP unit produced more electricity and heat in Strasbourg. However, this led to the higher biomass fuel use in Strasbourg but, as compensation, the received solar energy fuel was lower than in Barcelona. In Barcelona, this was the other way around. Additionally, the amount of the PVT electricity product was higher but the amount of the heat exergy products was lower due to the lower heating demand and the higher monthly reference temperatures.

The overall exergy efficiency of the same HRES in different locations can be close to each other because of the different component utilization rates and varying exergy of the heat products depending on the reference temperature. In terms of the PVT collectors, the decreased value of the heat products is compensated by the increased amount of PVT electricity production due to the higher solar radiation.

Next, the results of the exergo-economic analysis will be presented and discussed.

3.2. Exergo-economic analysis

The exergo-economic costs of the electricity produced by the HRES in each location are presented in Fig. 13. The specific cost of the system electricity takes into account the specific costs of the PVT and micro-CHP electricity according to Eq. (40). Figure 11 shows the specific cost of electricity cumulated on a monthly and yearly basis. The specific costs varied strongly in each location over the year with the minimum value as low as 0.189 €/kWh (or kWh_{ex} as electricity is seen as pure exergy) in each location during the summer and as high as 0.798 €/kWh in Tampere, Finland in November. In each location, the costs were lowest during the summer months when the PVT field produced most of the electricity. During the winter months, the costs increased in each location due to a greater share of the electricity produced by the micro-CHP, which had the higher initial investment cost, existing fuel costs and lower nominal electrical power. However, in Barcelona, the monthly specific costs were 15 to 30 c€/kWh lower during the winter months than in Strasbourg and France due to the better availability of solar energy.

Figure 13 shows that the specific cost of electricity was surprisingly close to each other in Strasbourg and Tampere when taking into account the physical distance between the locations. However, from November to January, the solar share of the electricity production was lower in Tampere resulting in over 10c€/kWh higher specific cost of electricity. The specific costs in Tampere and Strasbourg were close to Barcelona only during the best months of solar radiation, and during the rest of the year, the costs were 16% to 43% lower in Barcelona than in two other locations.

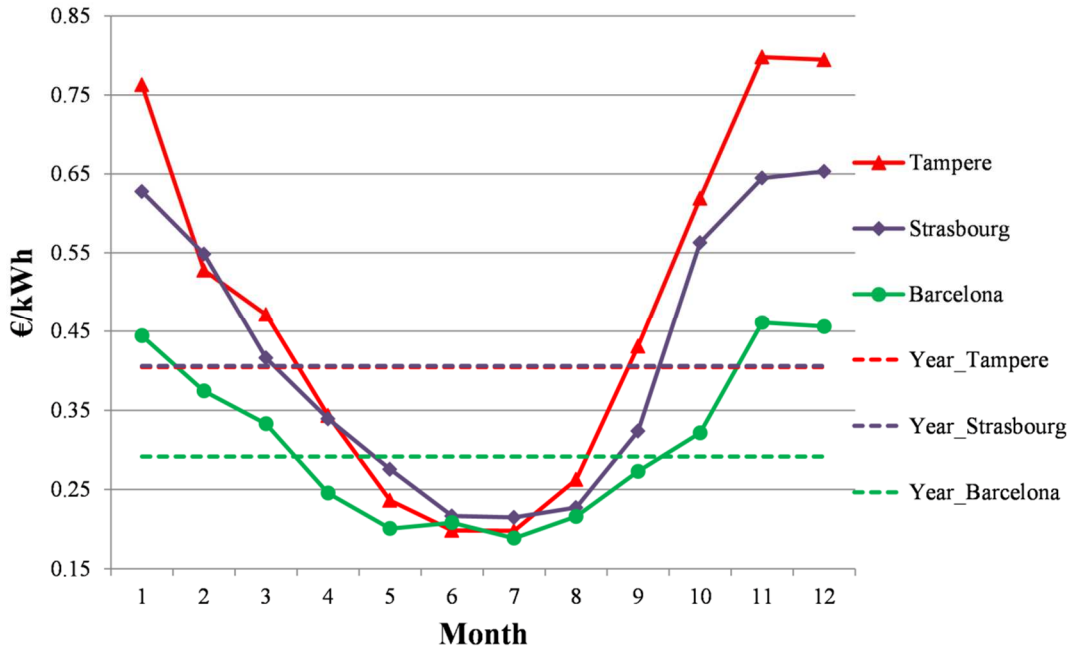

Fig. 13. The monthly and yearly exergo-economic costs of electricity produced by the hybrid energy system in Tampere, Strasbourg and Barcelona.

The results in Fig. 13 reveal that the available solar support from the PVT field decreased the specific cost of electricity significantly compared to the months, such as January and February, when the micro-CHP run almost at full requirements due to low solar irradiation and high space heating demand. In Tampere, the specific cost was reduced by 75%, by 66% in Strasbourg and by 59% in Barcelona due to increased solar support between the winter and summer. The impact of the solar support on the costs was also seen in the annual specific cost of electricity presented in Fig. 11. These costs were the lowest in sunny Barcelona resulting in 0.292 €/kWh and the highest in Strasbourg with 0.406 €/kWh. The annual specific cost was only slightly lower in Tampere than in Strasbourg with 0.404 €/kWh although the highest monthly specific cost were resulted in Tampere.

In Fig. 14 is presented the exergo-economic specific cost of space heating in each location on monthly and early basis.

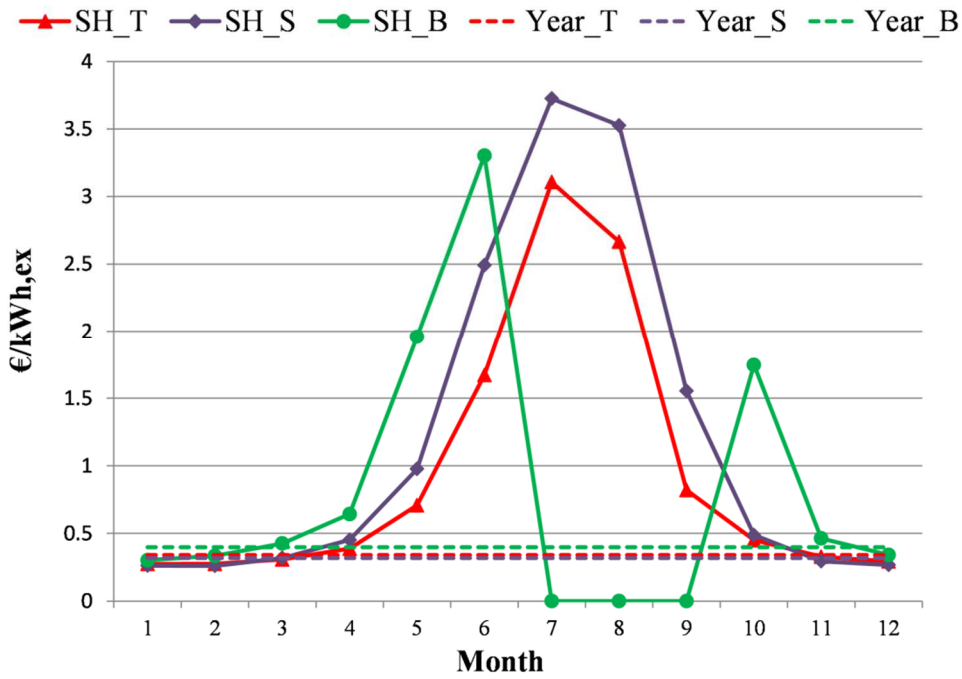

Fig. 14. The monthly and yearly exergo-economic costs of space heating in Tampere, Strasbourg and Barcelona.

The exergo-economic cost of the space heating reached the highest value of 3.73 €/kWh$_{ex}$ in Strasbourg in July due to low space heating demand and high ambient temperature. At the same time, the cost reached the highest value in Tampere as well with 3.11 €/kWh$_{ex}$. In Barcelona, there was no space heating demand from July to September and the specific cost was zero. Figure 14 shows that the specific cost reached the highest values in Barcelona and lowest in Tampere over the year. This was caused by the higher space heating demand and cooler reference temperatures in Tampere which leads to higher heat exergy production.

Figure 14 presents the specific cost of space heating per kWh of exergy, not energy. Based on the monthly energy levels of the heat exergy flows, the cost transfer coefficient of thermal exergy to energy varied from 0.143 to 0.068 in Tampere, from 0.115 to 0.061 and 0.095 to 0.054 in Strasbourg and Barcelona, respectively. The energy levels of the exergy flows were highest during the cooler months. The annual average specific cost of space heating was the highest in Barcelona with 0.399 €/kWh$_{ex}$ which resulted in 0.036 €/kWh. In Tampere and Strasbourg, the costs were slightly lower in terms of exergy resulting in 0.341 €/kWh$_{ex}$ (0.044 €/kWh) and 0.319 €/kWh$_{ex}$ (0.034 €/kWh), respectively.

In Fig. 15 is presented the exergo-economic cost of DHW in each location on monthly and yearly basis. The DHW profile was assumed to be the same in each location but the specific cost of DHW were influenced also by the current space heating demand. Due to that, the specific cost reached a value as high as 11.9 €/kWh$_{ex}$ in Barcelona in August when the space heating demand was zero and all costs were allocated only to the DHW. At the same time, the specific costs were 60% lower in Strasbourg and 74% lower in Tampere.

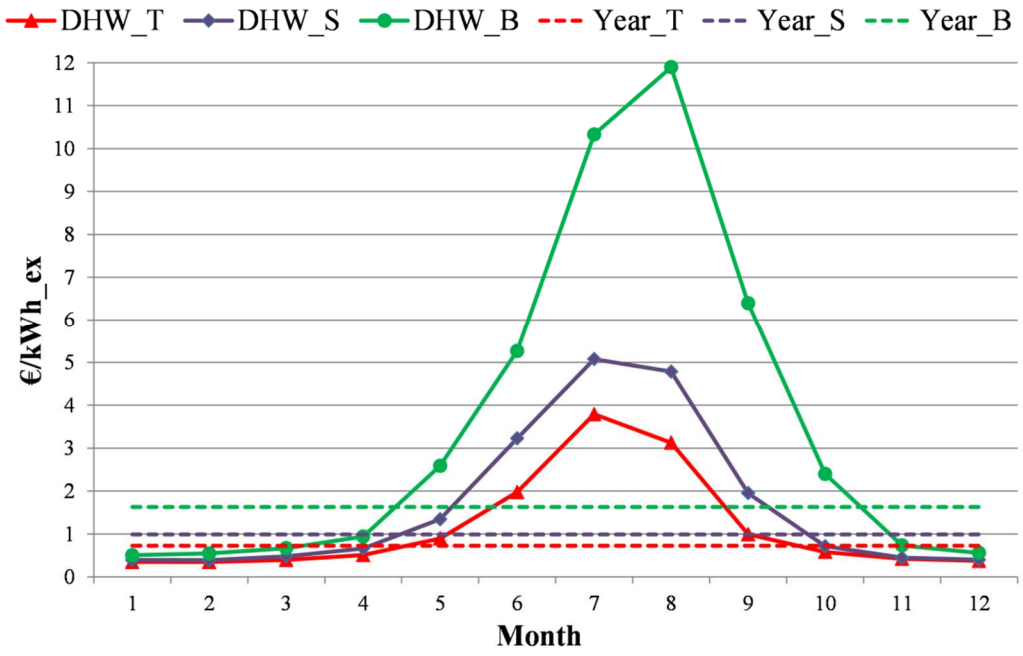

Fig. 15. The monthly and yearly exergo-economic costs of DHW in Tampere, Strasbourg and Barcelona.

On yearly basis, the specific cost of the DHW was the highest in Barcelona with 1.626 €/kWh$_{ex}$ which resulted in 0.111 €/kWh. In Strasbourg and Tampere, the costs were lower resulting in 0.987 €/kWh$_{ex}$ (0.083 €/kWh) and 0.725 €/kWh$_{ex}$ (0.075 €/kWh), respectively.

In this study, the exergo-economic calculation took into account the energy level of the exergy flows in order to allocate more production costs to an energy product with the higher energy level. Due to this, the specific cost of DHW were higher than the specific cost of space heating which had the lower temperature and energy level than the DHW. On the other hand, the specific cost of electricity was the highest among the energy products of the system because of the highest energy level of 1 as electricity is seen as pure exergy. It should be also noted that this study was conducted not taken into account any renewable energy based support or incentive mechanism. However, when comparing different countries, this study took into account the country specific tax and prices in Table 5.

Based on the performed exergo-economic analysis it can be concluded that the reasonable unit prices assigned to each energy product of the HRES differ according to the location and climate conditions of the hybrid system. These prices are presented in Table 5.

Table 5. The average unit prices of the energy products in each location.

Energy product	Barcelona	Strasbourg	Tampere	Unit
Electricity	0.292	0.406	0.404	€/kWh = €/kWh$_{ex}$
Space heating	0.036	0.034	0.044	€/kWh
	0.399	0.319	0.341	€/kWh$_{ex}$
Domestic hot water	0.111	0.083	0.075	€/kWh
	1.626	0.987	0.725	€/kWh$_{ex}$

It can be recognized that the appropriate electricity prices are relatively high compared to the country-specific electricity purchase prices in Table 6. This is mainly caused by the high initial investment of the HRES. At the moment, it is not realistic to gain the electricity prices above by selling or self-consuming the produced electricity of the HRES. However, the investment costs of the components can be expected to be reduced in the future while the grid electricity prices are expected to increase. Additionally, a thermally activated cooling

device could be added to the system to increase the utility of the system during the summer months and decrease the prices of the heat products.

3.2.1. Sensitivity analysis of exergo-economics

The sensitivity analysis was conducted to investigate the impact of the solar and storage component capacities on the exergo-economic costs. The exergo-economic results in Strasbourg were used as a reference in the analysis. First, the number of the PVT rows was decreased and increased by 33% by removing and adding one row to the original system configuration presented in Section 2. Varying the number of PVT collectors had a strong impact on the monthly and annual specific cost of the electricity as shown in Fig. 16.

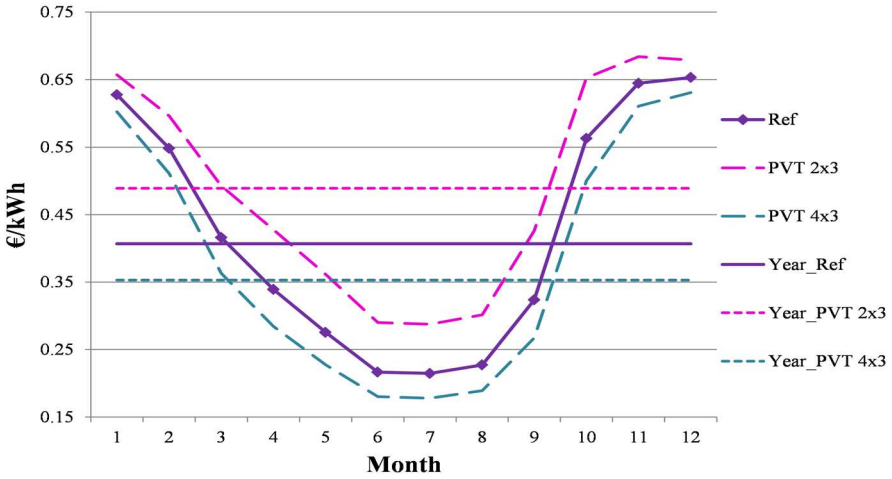

Fig. 16. The monthly and yearly exergo-economic costs of electricity produced by the hybrid energy system with different PVT capacities.

Decreasing the number of PVT collectors increased the monthly and annual specific cost of electricity because the cost-free solar fuel was reduced and compensated by the costly biomass fuel to cover energy demand. Adding the PVT collectors resulted in the opposite results but with a lower magnitude. The smaller PVT field increased the annual specific cost of electricity by 20% while the larger field decreased the cost by 13%. In terms of the space heating and DHW, varying the number of the PVT collectors did not influence the specific cost because these heat products were not the direct output of the PVT field but the thermal storage.

Next, the thermal storage volume was varied by ±25% compared to the reference system resulting in the storage sizes of 1.5 m^3 and 2.5 m^3. The thermal storage is used to facilitate the matching between thermal energy production and demand. Varying the storage size had an impact on the initial investment cost but not on the magnitude of the heat products defined by the building energy use. Due to this, the monthly specific costs of the heat product were increased or decreased only during the summer months when the heating demand was relatively low as shown in Fig. 17.

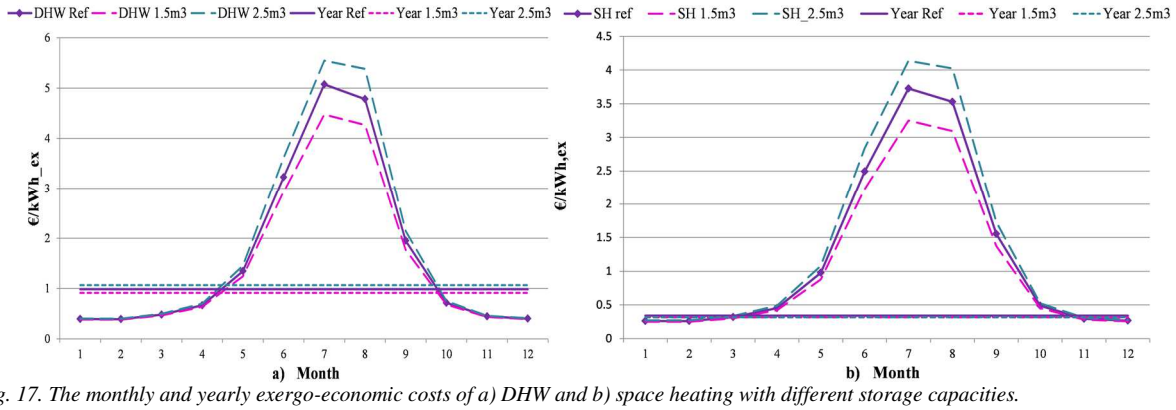

Fig. 17. The monthly and yearly exergo-economic costs of a) DHW and b) space heating with different storage capacities.

In July and August, the specific costs of DHW were 9.3% and 12.6% higher, respectively, if the size was increased. Decreasing the size led to 11.7% and 10.7% lower DHW costs in these months. The variation in the specific cost of space heating was with the same magnitude. The storage size did not influence the specific cost of electricity.

3.3. Comparative results of the HRES to the reference system

Energy, exergy and economic comparison indicators were used to further evaluate the performance of the cogeneration based HRES compared to separated production of heat and power by a reference system. The primary energy savings (PES) were used as an energetic indicator, the relative avoided irreversibility (RAI) as an exergetic indicator, and the simple payback time and net present value as economic indicators.

In terms of PES and RAI indicators, the reference system included an electric grid with an efficiency of 35% for electricity and a natural gas-fired boiler with an efficiency of 80% for heat production. In Fig. 18 is presented the monthly PES in each location compared to the reference system. The primary energy savings took into account only the reduction in biomass use because solar energy is CO_2 and cost-free primary energy. Figure 18 shows significantly high primary energy savings in each location during the sunniest months from May to August, when the PES was over 60% in each location. The system operation in Barcelona resulted in the highest PES over the year leading to the PES of over 90% from May to September. The PES values were almost the same during the year in Tampere and Strasbourg despite September when the PES was 68% in Strasbourg and 40% in Tampere due to strongly reduced solar irradiation in the northern location.

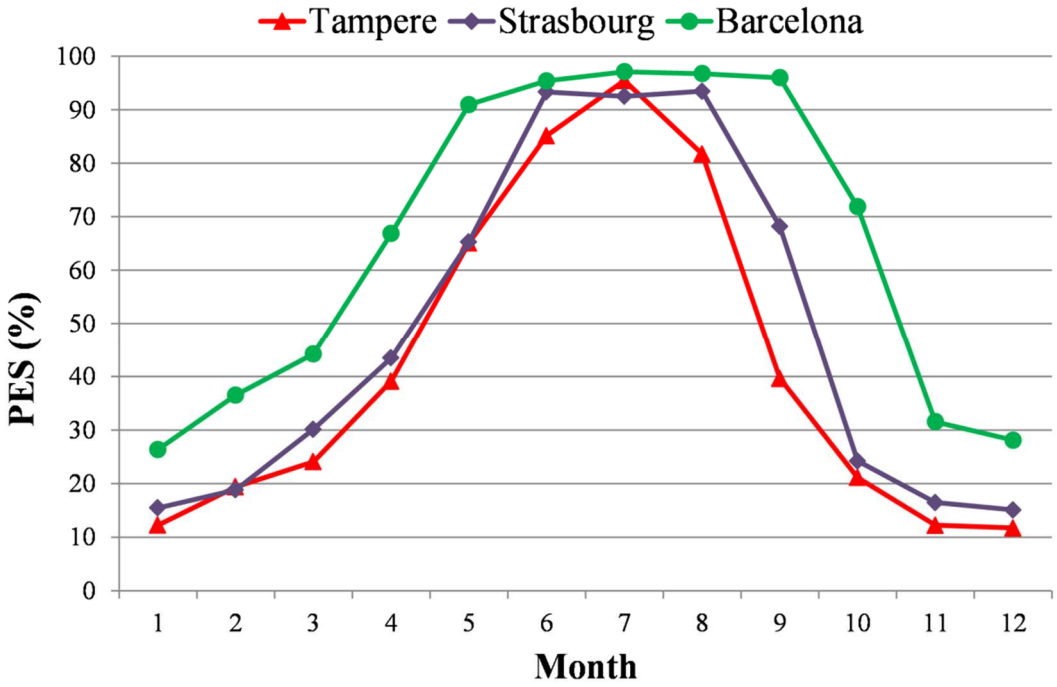

Fig. 18. The monthly primary energy savings in each location.

In each location, the PES was positive and primary energy was saved during the whole year. Based on the results, it can be concluded that hybridization of the fuel-fired micro-CHP system with solar cogeneration reduced strongly primary energy use compared to the reference system. In terms of exergy, the monthly RAI indicator showed the existing irreversibility savings in the HRES compared to the reference system but always at the lower level than primary energy savings. However, in Fig. 19, the RAI indicator revealed inefficiency of the HRES in Tampere in November when the RAI got a negative value. This indicates that the HRES was not an improvement from the reference system in November. In Tampere and Strasbourg, the RAI indicator was negative or close to zero from November to January. This was mainly caused by the low solar energy production. As a conclusion, the RAI indicator revealed the hidden inefficiency of the HRES operation which was not seen in the PES indicator.

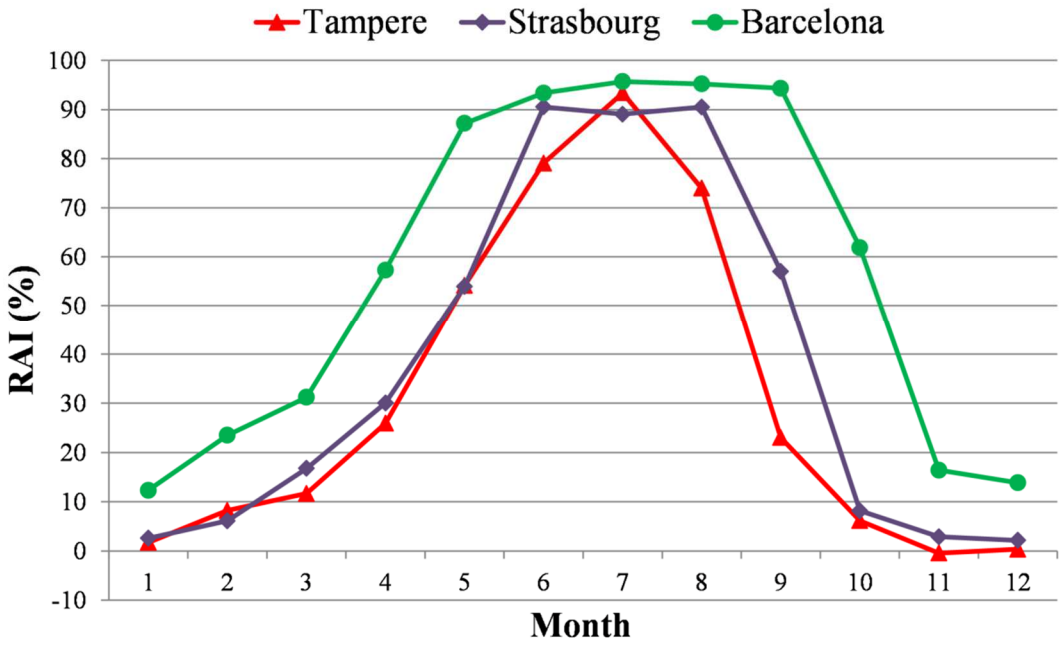

Fig. 19. The monthly relative avoided irreversibility in each location.

Next, the economic indicators were calculated for four different scenarios in each location. The SPT and NPV of the HRES are presented in Table 6 with the country-specific parameters used in the calculation. These economic calculations were conducted for the replacement of the reference system by the HRES. The case 1 compared the HRES to the reference system including the electric grid and natural gas boiler, and the case 2 compared to the reference system consisting only of the electric grid. Within the cases, the following two sub-scenarios were considered: a) dynamic electricity balance between the load and production was taken into account, and b) all produced electricity was assumed to be consumed by the building. In the sub-scenario a), the produced electricity was consumed in the building according to the load profile in Section 2.3 and the surplus production was fed to the grid with the country-specific feed-in-tariff presented in Table 6. The sub-scenario b) presented an ideal situation to show how the economic indicators were changed if the perfect match between the load and production would be possible.

Table 6. The parameters used in the economic comparison to the reference systems and economic results in each location.

	Tampere	Strasbourg	Barcelona	Ref.
Electricity demand	6000 kWh/year	6000 kWh/year	6000 kWh/year	
Heating demand	22475 kWh/year	24571 kWh/year	12901 kWh/year	
DHW	4238 kWh/year	4238 kWh/year	4238 kWh/year	
Electricity price	0.174 €/kWh	0.19 €/kWh	0.224 €/kWh	[45]
Natural gas price	0.087 €/kWh	0.075 €/kWh	0.09 €/kWh	[46,47]
Wood pellet price	0.27 €/kg	0.25 €/kg	0.23 €/kg	[48]
Feed-in-Tariff	0 €/kWh	0.06 €/kWh	0.05 €/kWh	[49–51]
VAT	24%	20%	21%	
	Tampere	Strasbourg	Barcelona	
RESULTS				
Savings, case 1a	1 830 €/year	1 887 €/year	1 939 €/year	
SPT, case 1a	19.3 years	18 years	17.7 years	
NPV, case 1a	508 €	2 781 €	6 585 €	
Savings, case 1b	2 217 €/ year	2 212 €/year	2 435 €/year	
SPT, case 1b	15.9 years	15.4 years	14.1 years	
NPV, case 1b	8 054 €	9 105 €	3 474 €	

Savings, case 2a	3 361 €/year	4 525 €/year	3 748 €/year
SPT, case 2a	10.5 years	7.5 years	9.2 years
NPV, case 2a	30 388 €	54 243 €	38 803 €
Savings, case 2b	3 747 €/year	4 848 €/year	4 245 €/year
SPT, case 2b	9.4 years	7 years	8.1 years
NPV, case 2b	37 934 €	60 567 €	48 494 €

The economic indicators in Table 6 show that the retrofitting of the old system with the considered HRES had economic viability under given circumstances in each location. The NPV was positive in each location after 25 years period. The longest simple payback time was indicated for the case 1a in Tampere resulting in 19.3 years with the NPV of only 508 €. This case took into account the dynamic behaviour of the electricity production and demand which is rarely matched with each other without energy storage. In this case, the surplus electricity was sold to the grid with the country-specific feed-in-tariff. The SPT was decreased by 3.4 years if the produced electricity was assumed to be used totally in the building. Additionally, the NPV was increased by 7546 €. In the case 1a, the SPT was 1.3 and 1.6 years shorter in Strasbourg and Barcelona, respectively, than in Tampere due to more favourable economic conditions, such as the feed-in-tariff and VAT.

The economic viability of retrofitting the electricity only based system (case 2) by the HRES resulted in significantly shorter SPT than in the case 1. In Tampere, the SPT of the case 2a was 10.5 years with the NPV of 30388 €. The shortest SPT of the case 2 was indicated in Strasbourg due to lower electricity price combined with low VAT for the initial investment. Assuming the 100% self-consumption in the building resulted only in a small reduction of the SPT. However, the reduction was less significant than between the case 1a and 1b.

The economic results revealed the higher viability of the hybrid system if the produced electricity was used 100% on-site. The electrical energy storage or electric car with advanced and intelligent system control can facilitate the energy management of the system and enable 100% self-consumption but increases the initial investment costs as well.

4. Conclusion

In this paper, a hybrid renewable energy system based on cogeneration from biomass-fuelled Stirling engine micro-CHP unit and photovoltaic-thermal collectors was assessed thermo-economically under three different European climate and economic conditions. The dynamic exergy and exergo-economic analyses were performed and the results were presented on a daily, monthly and yearly basis.

Compared to a yearly analysis, the conducted dynamic exergy analysis gives more detailed insight to the variation of exergy fuels, products and efficiency over the year. The dynamic exergo-economic analysis reveals the high variation in the specific cost of energy products compared to the yearly analysis. This variation is mainly caused by the fluctuating solar energy availability and heat demand of the reference building.

The location of the HRES had an impact on the following issues: the utilization rate of the energy production units within the system, exergy of the heat products, heating demand of the building, economic conditions, payback time, specific costs of energy products, primary energy savings and relative avoided irreversibility. The location of the HRES did not influence significantly the overall exergy efficiency of the system.

First, the results were obtained in terms of monthly fuel exergy, exergy destruction in the components, exergy products and the overall exergy efficiency. The following main findings were done:

- The share of solar exergy was the highest during the summer period in each location. In the southernmost location of Barcelona, the share was also significant during the winter months from November to March covering at worst 26% of fuel exergy in January.
- The micro-CHP caused most of the exergy destruction during the winter months while the PVT dominated the destruction during the summer months. The TES caused 2.5%-6% of the total monthly exergy destruction.
- The hybridization increased significantly cost-free electricity production and facilitated to reduce biomass use and costly exergy destruction during the whole year in each location.
- The overall exergy efficiency of the system varied from 13% to 16% over the year.

762
763 The following main findings were done based on the exergo-economic analysis:
764 - The specific cost of electricity varied strongly in each location over the year with the minimum value
765 as low as 0.189 €/kWh in each location during the summer months and as high as 0.798 €/kWh in
766 Tampere, Finland in November.
767 - The lowest specific cost of electricity is competitive with the current grid electricity prices in Table 6
768 which makes the system attractive for the building owner (prosumer).
769 - The annual specific cost of electricity was 28% lower in Barcelona (0.292 €/kWh) than in Strasbourg
770 (0.406 €/kWh) and Tampere (0.404 €/kWh) due to the higher utilization rate of the PVT and the lower
771 rate of the costly micro-CHP unit, and more favourable economic conditions. The similar utilization
772 rate of the PVT, less favourable economic conditions of Finland and higher exergy of heat products in
773 Finland resulted in the same annual specific cost of electricity in Tampere and Strasbourg.
774 - The specific cost of the space heating varied over year depending on the heating demand by having the
775 highest value of 3.73 €/kWh$_{ex}$ in July in Strasbourg and the lowest value of 0.26 €/kWh$_{ex}$ in January.
776 - The DHW had the highest monthly costs of 11.9 €/kWh$_{ex}$ in Barcelona in August due to the highest
777 reference temperature and the lowest space heating demand. The lowest cost were 0.35 €/kWh$_{ex}$ in
778 January in Tampere. The cost of the DHW was higher than space heating due to higher exergy content.
779 - The specific cost of electricity was sensitive to the number of the PVT collectors but not to the size of
780 the thermal storage. The 33% smaller PVT field increased the annual specific cost by 20% while the
781 33% larger field decreased the cost by 13%.
782
783 Finally, the HRES was compared against two reference systems including the electric grid with or without a
784 gas boiler. Additionally, the self-consumption rate of the produced electricity was taken into account and varied
785 within two reference cases. The following main findings were done:

786 - The hybridization reduced primary energy use and irreversibility up to 95% compared to the reference
787 system.
788 - The longest SPT of 19.3 years resulted in Tampere and the shortest in Barcelona of 14.1 years if the
789 comparison was made against the electric grid combined with a natural gas boiler. If only the electric
790 grid was considered as a reference system, the SPT was between 7 to 10.5 years depending on the
791 scenario and location.
792 - The HRES was economically viable in each case while the NPV resulted to be positive.
793 - The economic results revealed the higher viability of the HRES if the produced electricity was used
794 100% on-site.
795
796 To enhance the matching of renewable energy production and building energy demand, the upcoming future
797 work should include an investigation of integrating battery storage or electric vehicle into the system with the
798 Time-of-Use tariff. Additionally, the optimization of the energy demand side and the HRES will be performed
799 for each location. More research on advanced and intelligent energy management algorithms is required as well
800 to control better the energy flows in the hybrid renewable energy system.
801

802 **Acknowledgements**

803 The authors would like to thank Interreg V Rhin supérieur ACA-MODES project for their support and
804 funding of this research.
805

806 **References**

807 [1] E. Doroudchi, K. Alanne, Ö. Okur, J. Kyyrä, M. Lehtonen, Approaching net zero energy housing through integrated
808 EV, Sustain. Cities Soc. 38 (2018) 534–542. https://doi.org/10.1016/j.scs.2018.01.042.
809 [2] European Comission, Energy performance of buildings directive, (n.d.). https://ec.europa.eu/energy/topics/energy-
810 efficiency/energy-efficient-buildings/energy-performance-buildings-directive_en.
811 [3] Eurostat, Eurostat, Online Publ. Eurostat. (2020). https://ec.europa.eu/eurostat/statistics-

812 explained/index.php?title=Energy_efficiency_statistics#Primary_energy_consumption_and_distance_to_2020_and_
813 2030_targets (accessed January 19, 2022).
814 [4] EU Building Factsheets, (n.d.). https://ec.europa.eu/energy/eu-buildings-factsheets_en.
815 [5] S.B. Sadineni, S. Madala, R.F. Boehm, Passive building energy savings: A review of building envelope
816 components, Renew. Sustain. Energy Rev. 15 (2011). https://doi.org/10.1016/j.rser.2011.07.014.
817 [6] V. Palomba, E. Borri, A. Charalampidis, A. Frazzica, L.F. Cabeza, S. Karellas, Implementation of a solar-biomass
818 system for multi-family houses: Towards 100% renewable energy utilization, Renew. Energy. 166 (2020) 190–209.
819 https://doi.org/10.1016/j.renene.2020.11.126.
820 [7] S. Murugan, B. Horák, A review of micro combined heat and power systems for residential applications, Renew.
821 Sustain. Energy Rev. 64 (2016) 144–162. https://doi.org/10.1016/j.rser.2016.04.064.
822 [8] European Comission, European Comissions, Energy Efficiency Directive 2012/27/EU, (n.d.). https://eur-
823 lex.europa.eu/legal-content/EN/TXT/PDF/?uri=CELEX:32012L0027&from=EN.
824 [9] A.C. Ferreira, J. Silva, S. Teixeira, J.C. Teixeira, S.A. Nebra, Assessment of the Stirling engine performance
825 comparing two renewable energy sources: Solar energy and biomass, Renew. Energy. 154 (2020) 581–597.
826 https://doi.org/10.1016/j.renene.2020.03.020.
827 [10] P. Bajpai, V. Dash, Hybrid renewable energy systems for power generation in stand-alone applications: A review,
828 Renew. Sustain. Energy Rev. 16 (2012) 2926–2939. https://doi.org/10.1016/j.rser.2012.02.009.
829 [11] R. Figaj, Performance assessment of a renewable micro-scale trigeneration system based on biomass steam cycle,
830 wind turbine, photovoltaic field, Renew. Energy. 177 (2021) 193–208.
831 https://doi.org/10.1016/J.RENENE.2021.05.143.
832 [12] L. Romero Rodríguez, J.M. Salmerón Lissén, J. Sánchez Ramos, E.Á. Rodríguez Jara, S. Álvarez Domínguez,
833 Analysis of the economic feasibility and reduction of a building's energy consumption and emissions when
834 integrating hybrid solar thermal/PV/micro-CHP systems, Appl. Energy. 165 (2016) 828–838.
835 https://doi.org/10.1016/j.apenergy.2015.12.080.
836 [13] J.M. Pearce, Expanding photovoltaic penetration with residential distributed generation from hybrid solar
837 photovoltaic and combined heat and power systems, Energy. 34 (2009) 1947–1954.
838 https://doi.org/10.1016/J.ENERGY.2009.08.012.
839 [14] A.S. Mundada, K.K. Shah, J.M. Pearce, Levelized cost of electricity for solar photovoltaic, battery and cogen
840 hybrid systems, Renew. Sustain. Energy Rev. 57 (2016) 692–703. https://doi.org/10.1016/j.rser.2015.12.084.
841 [15] J. Settino, P. Morrone, A. Algieri, T. Sant, C. Micallef, M. Farrugia, C. Spitieri-Staines, J. Licari, A. Micallef,
842 Integration of an Organic Rankine Cycle and a Photovoltaic Unit for Micro-Scale CHP Applications in the
843 Residential Sector, in: Energy Procedia, Elsevier Ltd, 2017: pp. 597–604.
844 https://doi.org/10.1016/j.egypro.2017.08.223.
845 [16] J. Facão, A. Palmero-Marrero, A.C. Oliveira, Analysis of a solar assisted micro-cogeneration ORC system, Int. J.
846 Low-Carbon Technol. 3 (2008) 254–264. https://doi.org/10.1093/IJLCT/3.4.254.
847 [17] J. Kotowicz, W. Uchman, Analysis of the integrated energy system in residential scale: Photovoltaics, micro-
848 cogeneration and electrical energy storage, Energy. 227 (2021) 120469.
849 https://doi.org/10.1016/j.energy.2021.120469.
850 [18] J.A. Auñón-Hidalgo, M. Sidrach-de-Cardona, F. Auñón-Rodríguez, Performance and CO2 emissions assessment of
851 a novel combined solar photovoltaic and thermal, with a Stirling engine micro-CHP system for domestic
852 environments, Energy Convers. Manag. 230 (2021) 113793. https://doi.org/10.1016/j.enconman.2020.113793.
853 [19] S. Kallio, M. Siroux, Hybrid renewable energy systems based on micro-cogeneration, Energy Reports. 8 (2022)
854 762–769. https://doi.org/10.1016/J.EGYR.2021.11.158.
855 [20] A. Mouaky, A. Rachek, Energetic, exergetic and exergeoeconomic assessment of a hybrid solar/biomass
856 poylgeneration system: A case study of a rural community in a semi-arid climate, Renew. Energy. 158 (2020) 280–
857 296. https://doi.org/10.1016/j.renene.2020.05.135.
858 [21] F. Calise, M. Dentice d'Accadia, A. Piacentino, Exergetic and exergoeconomic analysis of a renewable
859 polygeneration system and viability study for small isolated communities, Energy. 92 (2015) 290–307.
860 https://doi.org/10.1016/j.energy.2015.03.056.
861 [22] J. Wang, Y. Chen, N. Lior, Exergo-economic analysis method and optimization of a novel photovoltaic/thermal
862 solar-assisted hybrid combined cooling, heating and power system, Energy Convers. Manag. 199 (2019).
863 https://doi.org/10.1016/j.enconman.2019.111945.
864 [23] A. Wohlfeil, CARNOT Toolbox. FH Aachen., CARNOT Toolbox. (2019). https://fh-
865 aachen.sciebo.de/index.php/s/0hxub0iIJrui3ED (accessed December 14, 2020).
866 [24] B. Hafner, J. Plettner, C. Wemhöner, W. Thomas, CARNOT Blockset Version 1.0, 1999.

[25] S. Kallio, M. Siroux, Energy Analysis and Exergy Optimization of Photovoltaic-Thermal Collector, Energies. 13 (2020) 5106. https://doi.org/10.3390/en13195106.
[26] I. Beausoleil-Morrison, An Experimental and Simulation-Based Investigation of the Performance of Small-Scale Fuel Cell and Combustion-Based Cogeneration Devices Serving Residential Buildings Energy Conservation in Buildings and, 2008. www.ecbcs.org.
[27] K. Alanne, N. Söderholm, K. Siŕen, Implementation and validation of combustion engine micro-cogeneration routine for the simulation program IDA-ICE, IBPSA 2009 - Int. Build. Perform. Simul. Assoc. 2009. (2009) 33–40.
[28] K. Lombardi, V.I. Ugursal, I. Beausoleil-Morrison, Proposed improvements to a model for characterizing the electrical and thermal energy performance of Stirling engine micro-cogeneration devices based upon experimental observations, Appl. Energy. 87 (2010) 3271–3282. https://doi.org/10.1016/j.apenergy.2010.04.017.
[29] Equa, IDA Indoor Climate and Energy, (n.d.). https://www.equa.se/en/ida-ice.
[30] U. Jordan, K. Vajen, Influence of the DHW profile on the Fractional Energy\rSavings: A Case Study of a Solar Combi-System, Sol. Energy. 69(Suppl.) (2000) 197–208.
[31] U. Jordan, K. Vajen, DHWcalc: Program to generate Domestic Hot Water profiles with statistical means for user defined conditions, in: Proc. Sol. World Congr. 2005 Bringing Water to World, Incl. Proc. 34th ASES Annu. Conf. Proc. 30th Natl. Passiv. Sol. Conf., 2005: pp. 1525–1530. www.solar.uni-kassel.de. (accessed September 3, 2021).
[32] BDEW, Standardlastprofile Strom, (n.d.). https://www.bdew.de/energie/standardlastprofile-strom/ (accessed December 18, 2020).
[33] F. (2012) Kottek, M. & Rubel, Updated Köppen-Geiger climate classification, (n.d.). http://koeppen-geiger.vu-wien.ac.at/present.htm.
[34] ASHRAE, ASHRAE IWEC, (n.d.). https://www.ashrae.org/technical-resources/bookstore/ashrae-international-weather-files-for-energy-calculations-2-0-iwec2.
[35] Equa, ASHRAE IWEC weather files, (n.d.). http://www.equaonline.com/ice4user/new_index.html.
[36] R.M. da Silva, J.L.M. Fernandes, Hybrid photovoltaic/thermal (PV/T) solar systems simulation with Simulink/Matlab, Sol. Energy. 84 (2010) 1985–1996. https://doi.org/10.1016/j.solener.2010.10.004.
[37] P. Gonçalves, G. Angrisani, C. Roselli, A.R. Gaspar, M.G. Silva, L.R. Santos, Energy and exergy-based modeling and evaluation of a micro-combined heat and power unit for residential applications, in: 3 Microgen, 2013.
[38] M. Gong, G. Wall, Exergy Analysis of the Supply of Energy and Material Resources in the Swedish Society, Energies. 9 (2016) 707. https://doi.org/10.3390/en9090707.
[39] A. Farzanehnia, M. Sardarabadi, Exergy in Photovoltaic/Thermal Nanofluid-Based Collector Systems, Exergy Its Appl. - Towar. Green Energy Prod. Sustain. Environ. (2019). https://doi.org/10.5772/intechopen.85431.
[40] I.S. Ertesvåg, Exergetic comparison of efficiency indicators for combined heat and power (CHP), Energy. 32 (2007) 2038–2050. https://doi.org/10.1016/j.energy.2007.05.005.
[41] F. Calise, F.L. Cappiello, M. Dentice d'Accadia, M. Vicidomini, Thermo-economic optimization of a novel hybrid renewable trigeneration plant, Renew. Energy. 175 (2021) 532–549. https://doi.org/10.1016/J.RENENE.2021.04.069.
[42] A. Lazzaretto, G. Tsatsaronis, SPECO: A systematic and general methodology for calculating efficiencies and costs in thermal systems, Energy. 31 (2006) 1257–1289. https://doi.org/10.1016/J.ENERGY.2005.03.011.
[43] J. Wang, T. Mao, J. Wu, Modified exergoeconomic modeling and analysis of combined cooling heating and power system integrated with biomass-steam gasification, Energy. 139 (2017) 871–882. https://doi.org/10.1016/j.energy.2017.08.030.
[44] Tap water price, (n.d.). https://www.waternet.nl/en/service-and-contact/tap-water/costs/.
[45] Strom Report, Electricity Prices in Europe, (n.d.). https://strom-report.de/electricity-prices-europe/#electricity-prices-household-map (accessed November 24, 2021).
[46] Eurostat Statistics Explained, Natural gas prices for household consumers, (n.d.). https://ec.europa.eu/eurostat/statistics-explained/index.php?title=File:Natural_gas_prices_for_household_consumers,_second_half_2020_(EUR_per_kWh)_v1.png (accessed November 24, 2021).
[47] S. Kaasuenergia, Kaasulämmityksen hinnasto omakotitaloille, (n.d.). https://suomenkaasuenergia.fi/wp-content/uploads/2018/02/SK-Oy-ja-AK-Oy-Kotikulta-ja-Bio-Kotikulta-hinnasto.pdf (accessed November 24, 2021).
[48] C. Calderón, European Bioenergy Outlook, in: GreenGrain Proj. Conf., 2016: p. 15.
[49] Selectra, Autoconsumo con excedentes, (n.d.). https://selectra.es/autoconsumo/info/tarifas (accessed November 24, 2021).
[50] Commission de Régulation de l'Énergie, Le tarif de rachat photovoltaïque en 2021, (n.d.).

https://news.dualsun.com/aide-fiscalite/tarif-rachat-photovoltaique/ (accessed November 24, 2021).
[51] Motiva, Ylijäämäsähkön myynti, (n.d.). https://www.motiva.fi/ratkaisut/uusiutuva_energia/aurinkosahko/aurinkosahkojarjestelman_kaytto/ylijaamasahkon_myynti (accessed November 24, 2021).

Dynamic input profiles

Heating demand
Electiricty demand
Weather data

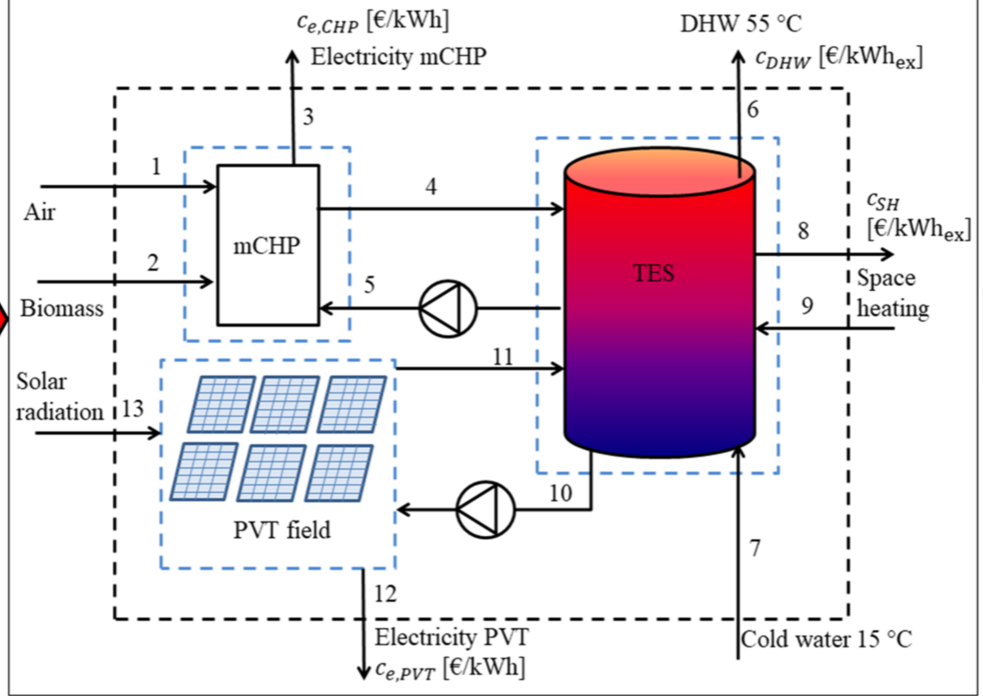

Dynamic output profiles

Exergy analysis
Exergy destruction
Exergy products
Exergy efficiency

Exergo-economic costs
Electricity
Space heating
Domestic hot water